EVALUATION OF DONOR ABILITIES OF NEUTRAL LIGANDS TO VANADIUM(V) NITRIDES

By

Linqing Mo

A THESIS

Submitted to
Michigan State University
in partial fulfillment of the requirements
for the degree of

Chemistry – Master of Science

2022

ABSTRACT

In catalyst design, the ancillary ligands play a crucial role in tuning the steric and electronic structure of the system and catalyst performance. Among those ancillary ligands, neutral ligands like phosphines (PR_3) or substituted pyridines are some of the most widely-used ligands in transition metal catalysis, making the study of the interaction between these ligands and the central metal necessary. While the interactions between phosphines and low oxidation state metals have been studied for decades, there are few studies concerning the interaction of those ligands with high oxidation state metals. For anionic ligands, our group has developed a new electronic parameter (Ligand Donor Parameter, LDP) using a chromium(IV) species. However, the exploration of neutral ligands with the same chromium species is not an effective method for measuring the neutral ligand donor ability. Computational studies of how neutral ligands will interact with high oxidation state metals will be presented in Chapter 2, in which a new vanadium(V) based model has been used. In Chapter 3, reactivity studies are described where we explored methods of preparing vanadium(V) complexes for donor ability measurements. These studies can give us a better understanding of neutral ligands' donor ability to the vanadium(V) metal center and extend our understanding of how these ligands interact to high oxidation state metals.

TABLE OF CONTENTS

LIST OF TABLES

LIST OF FIGURES

LIST OF SCHEMES

KEY TO SYMBOLS AND ABBREVIATIONS

LDP	Ligand Donor Parameter
IR	Infrared Radiation
TEP	Tolman Electronic Parameter ν
TCA	Tolman Cone Angle θ
Å	Angstrom
QALE	Quantitative Analysis of Ligand Effects
E_{ar}	The aromatic effect parameter
π_p	The π-acidic character
NMR	Nuclear Magnetic Resonance
e.u.	Entropy unit
$\Delta S^{\ddagger}$	Entropy of Activation
$\Delta H^{\ddagger}$	Enthalpy of Activation
$\%V_{bur}$	Percent Buried Volume
$BArF_{20}^-$	Tetrakis(2,3,4,5,6-fluoro-phenyl)borane
$BArF_{24}^-$	Tetrakis(3,5-(trifluoromethyl)phenyl)borane
DOSY	Diffusion Ordered Spectroscopy
NBO	Natural Bond Orbital
NRT	Natural Resonance Theory
ΔH°	Enthalpy of Protonation
χ	σ-donor Ability Parameter
θ	Tolman Cone Angle
LDP'_{calc}	Calculated Enthalpy Differences Between the Ground State and the Transition State

LDP'_{model}	Modeled Enthalpy Differences Between the Ground State and the Transition State
DFT	Density Functional Theory
NBO7	Natural Bond Orbital 7.0
THF	Tetrahydrofuran
py	Pyridine
4-^{t}bupy	4-*tert*-butylpyridine
quin	Quinuclidine
XRD	X-Ray Diffraction

Chapter 1. Introduction

1.1 Motivation

Catalysis plays a significant role in the modern chemical industry. Among these catalysts, high oxidation state metal center-based catalysts like titanium(IV) are widely used in both commodity chemicals, like polyolefins from Zeigler–Natta polymerization used to produce over 320 million tons polymers per year,[1] or specialty chemicals synthesized via Sharpless epoxidation.[2]

In catalyst design, the ancillary ligands play a crucial role because these ligands can strongly impact the electronic structure of the system and, in turn, catalyst performance. In those ancillary ligands, neutral ligands like phosphines are one of the most commonly used ligands in the organometallic catalysis field. Some examples include Grubbs catalyst used for olefin metathesis,[3] and a series of Pd and Ni phosphine complexes used for cross-coupling chemistry.[4] The reactivity of those catalysts can be significantly affected by the neutral ancillary ligands. For example, Grubbs "Generation 1" catalyst was found to be much more effective than the PPh_3 catalyst after replacing PPh_3 in $Ru(=CHPh)Cl_2(PPh_3)_2$ with PCy_3 groups (Scheme 1-1).[5]

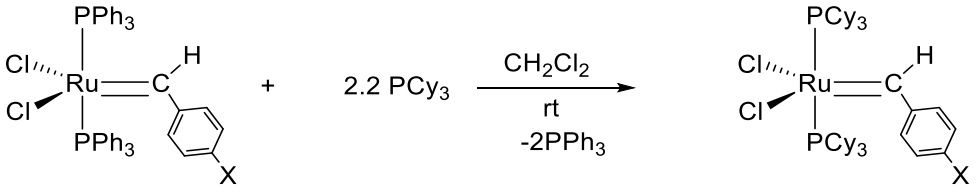

Scheme 1-1. Formation of the Grubbs "Generation 1" catalyst.

Unfortunately, researchers know little about the donor ability of neutral ligands towards high oxidation states metals, from both computational and applied chemistry. For people who are designing high oxidation state metal catalysts with neutral ligands, it would be helpful if there

was a tool that can predict the activity of the catalyst and aid in design of new catalysts guided by the electronic and steric properties of neutral ligands forward these metals.

1.2 Tolman's Cone Angle and Electronic Parameter

To better understand how neutral ligands affect the reactivity of a catalyst, researchers made great effort in determining their donor and steric properties. Perhaps one of the most notable early attempts in this area is the famous $Ni(CO)_3(PR_3)$ system developed by Chadwick Tolman.[6,7]

For this system, a series of $Ni(CO)_3(PR_3)$ complexes was synthesized. The A_1 stretching vibration of the C≡O bonds of those complexes was measured by IR spectroscopy and taken as the Tolman Electronic Parameter, ν(TEP). When the phosphine ligand PR_3 donates more electron density to the metal center Ni, the Ni will also donate more electron density into the π antibonding orbital of the CO ligands. So, as the phosphine becomes more donating, the TEP value will become lower. Usually, the very donating P^tBu_3 is scaled to 0 cm^{-1} as the reference of TEP.

The Tolman Cone Angle, θ(TCA), was measured by a simple but useful model. The space-filling calotte models of phosphine ligands were made. The steric parameter θ was obtained by measuring the apex angle of the cylindrical cone, centered 2.28 Å from the P atom, which touches the radii of the outermost atoms of the model (Figure 1-1).

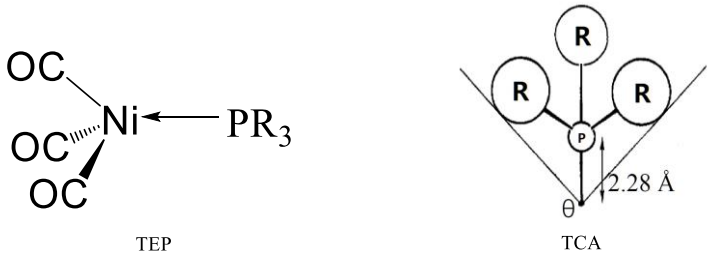

Figure 1-1. (left) The $Ni(CO)_3(PR_3)$ system Tolman used to determine the Tolman Electronic Parameter ν. (right) The CPK model for measuring Tolman Cone Angle θ.[7]

Tolman's two simple but beautiful assumptions were soon proved to be effective by regression analysis.

1.3 Quantitative Analysis of Ligand Effects (QALE)

The Quantitative Analysis of Ligand Effects (QALE) method was first developed by Giering.[8] After 20 years of development, it can separate different electronic and steric effects of a ligand and determine how important these effects can affect the reactivity.

Originally, the QALE model just included the TEP ν and TCA θ, but with the development of the method, new parameters were discovered and helped modify the accuracy of the system.[9-11] The method was improved by involving the aromatic effect parameter (E_{ar}) and the π-acidic character (π_p). By eliminating the contribution of the π-acceptor, the corrected TEP χ^d can represent the pure donor ability.[12] The E_{ar} is another corrected electronic parameter that depends on the number of non-alkyl substituents on the phosphine.[13,14]

The QALE method can also be applied to ligands other than phosphines and determine their stereoelectronic properties in great detail, like N-heterocyclic carbenes.[15]

Although the exploration of interactions between neutral ligands and low oxidation state metal centers has made great progress, when it comes to interactions with high oxidation state metals like vanadium(V) or chromium(VI), the study of parameterization methods has been neglected.

1.4 Ligand Donor Parameter (LDP)

For high oxidation state metal centers, the Odom group developed a new parameterization method in 2012.[16] This new system was based on $NCr(N^iPr_2)_2X$ complexes, where X is the ligand studied (Figure 1-2). In this new system, similar to Tolman's electronic parameter, the barriers of the Cr-N bond rotation in the complex were measured and taken as the Ligand Donor

Parameter, LDP. Because of the d^0 electronic structure of the metal center, the LDP value can better reflect the interaction between the high valent metal center and the ligand.

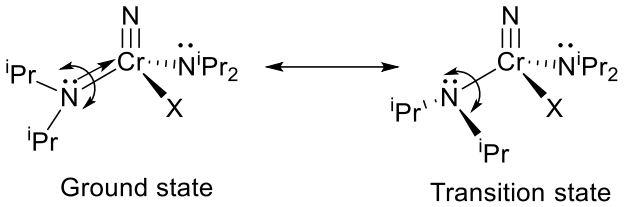

Figure 1-2. The chromium complex for the LDP study.

In those complexes, ligand X's σ- and π-donation towards the chromium center will compete with the donation from the lone pair electron density of the N^iPr_2 group. When ligand X is a poor donor, the π-accepter orbitals of Cr will accept more electron density from the N^iPr_2 group, creating more double bond character in the Cr-N bond. Conversely, the barrier to rotation will be lower if ligand X is a strong donor.

For measuring the barriers of the Cr-N bond rotation, the spin saturation transfer technique using ^{1}H NMR spectroscopy was applied.[17] In the Cr complex, the rotation of the Cr-N bond will have two chemical environments: the isopropyl group *syn* to the nitride or *anti* to the nitride, in which the septet protons will have different chemical shifts. After excitation of one septet, the rate of amide rotation can be calculated directly by the integration and the spin-relaxation time. By using the Eyring equation, the free energy to this rotation can be obtained.

By measuring the rate at different temperatures, it was found that $\Delta S^{\ddagger}$ values varied from -3 to -16 e.u.. Among those measurements, the most reliable value was from X=I, which was done over a 47 K interval. So, the entropy value of $NCr(N^iPr_2)_2I$ ($\Delta S^{\ddagger}$=-9 e.u.) was used as the standard value for LDP calculations. Based on this assumption, $\Delta H^{\ddagger}$ of the amide rotation was calculated by the Gibbs Equation, which was used as the Ligand Donor Parameter (LDP).

Like Tolman's parameterization method, a steric parameter, $\%V_{bur}$, was found to be useful to our modelling. The software developed by Cavallo and co-worker was used to model this parameter.[18] Imagine there is a sphere with a radius of 3.5Å around the chromium atom, the percentage of that sphere occupied by the ancillary ligand will be called $\%V_{bur}$. The LDP value and $\%V_{bur}$ can be combined to model high oxidation state metal catalysts. For example, detailed information on ligand properties in the hydroamination reaction catalyzed by the titanium(IV) system was modelled.[19]

1.5 LDP with Neutral Ligands

Over the years after the LDP system was established, the LDP values of a large series of anionic ligands were measured. Meanwhile, the evaluation of donor abilities of neutral ligands to high valent metals was ongoing. Attempts towards the application of neutral ligands in the Cr LDP system were published.[20,21]

In the first study, rare examples of $\{NCr(N^iPr_2)_2(PX_3)\}^+$ complexes, $\{NCr(N^iPr_2)_2(PMe_3)\}^+$ and $\{NCr(N^iPr_2)_2(PMe_2Ph)\}^+$, were synthesized.[20] The LDP measurement results showed that the ligand donor ability of these salts was sensitive to changes in solvents, except for some "noncoordinating" anions like $BArF_{20}^-$ and $BArF_{24}^-$, which had similar LDP values in $CDCl_3$ and CD_3CN. However, the ^1H DOSY NMR experiment showed that in nonpolar NMR solvents like $CDCl_3$, all counterions will ion-pair with the cation and interact with the alkyl group of the diisopropyl amide. In conclusion, the measurement of LDP in non-polar solvent will be affected by ion-pairing effects.

Since it might be practicable to use a polar solvent like CD_3CN as the NMR solvent, more varieties of $\{NCr(N^iPr_2)_2(PX_3)\}^+$ complexes were prepared.[21] But the LDP measurement results in CD_3CN showed that the entropy of the rotation barrier of those complexes spanned a large

range due to the solvent effects in polar solvents. Under this entropy range, the assumption that the entropy is a constant for LDP measurement can no longer be used. The special entropy value shown in the first study is a coincidence for the phosphine being used.

Due to the properties of chromium salts, the experimental studies of neutral ligands LDP in the chromium system seemed to be limited by ion-pairing effects and solvent effects. But these experimental and computational results showed that the interactions between neutral ligands and high valent metal centers were quite different from some late transition metals.

1.6 Conclusion Remarks

Due to the nature of the Cr salt complexes, there are still some problems that remain in the study of donor abilities of neutral ligands to high oxidation state metals. To overcome those experimental difficulties, a new neutral system with a similar structure to the Cr LDP system, $NV(NR_2)_2L$, was investigated. The oxidation state of the vanadium(V) center leads to the electronic neutrality of the whole complex, which can avoid the effect from counterions. In the following Chapter 2, computational studies of this system will be discussed, including interactions between ligands and the metal center, the bond patterns and resonance forms. In Chapter 3, some synthetic and characteristic data of some new vanadium imido complexes will be addressed.

REFERENCES

(1) Klosin, J.; Fontaine, P. P.; Figueroa, R. Development of Group IV Molecular Catalysts for High Temperature Ethylene-α-Olefin Copolymerization Reactions. *Acc. Chem. Res.* **2015**, *48* (7), 2004–2016.

(2) Sharpless, K. B. Searching for New Reactivity (Nobel Lecture). *Angew. Chem. Int. Ed.* **2002,** *41* (12), 2024.

(3) Nguyen, S. T.; Johnson, L. K.; Grubbs, R. H.; Ziller, J. W. Ring-Opening Metathesis Polymerization (ROMP) of Norbornene by a Group VIII Carbene Complex in Protic Media. *J. Am. Chem. Soc.* **1992**, *114* (10), 3974–3975.

(4) Johansson Seechurn, C. C. C.; Kitching, M. O.; Colacot, T. J.; Snieckus, V. Palladium-Catalyzed Cross-Coupling: A Historical Contextual Perspective to the 2010 Nobel Prize. *Angew. Chem. Int. Ed.* **2012**, *51* (21), 5062–5085.

(5) Grubbs, R. H. Olefin-Metathesis Catalysts for the Preparation of Molecules and Materials (Nobel Lecture). *Angew. Chem. Int. Ed.* **2006**, *45* (23), 3760–3765.

(6) Tolman, C. A. Electron Donor-Acceptor Properties of Phosphorus Ligands. Substituent Additivity. *J. Am. Chem. Soc.* **1970**, *92* (10), 2953–2956.

(7) Tolman, C. A. Steric Effects of Phosphorus Ligands in Organometallic Chemistry and Homogeneous Catalysis. *Chem. Rev.* **1977**, *77* (3), 313–348.

(8) Golovin, M. N.; Rahman, M. M.; Belmonte, J. E.; Giering, W. P. Quantitative Separation of .Sigma.- and .Pi.-Components of Transition Metal-Phosphorus Bonding and the Application of Ligand Effects in Organometallic Chemistry. *Organometallics* **1985**, *4* (11), 1981–1991.

(9) Rahman, M. M.; Liu, H. Y.; Prock, A.; Giering, W. P. Quantitative Analysis of Ligand Effects. 2. Steric and Electronic Factors Influencing Transition-Metal-Phosphorus(III) Bonding. *Organometallics* **1987**, *6* (3), 650–658.

(10) Eriks, K.; Giering, W. P.; Liu, H. Y.; Prock, A. Applications of the Quantitative Analysis of Ligand Effects (QALE). Steric Profiles for Reactions Involving "Spectator" Phosphorus(III) Ligands. *Inorg. Chem.* **1989**, *28* (9), 1759–1763.

(11) Rahman, M. M.; Liu, H. Y.; Eriks, K.; Prock, A.; Giering, W. P. Quantitative Analysis of Ligand Effects. Part 3. Separation of Phosphorus(III) Ligands into Pure .Sigma.-Donors and .Sigma.-Donor/.Pi.-Acceptors. Comparison of Basicity and .Sigma.-Donicity. *Organometallics* **1989**, *8* (1), 1–7.

(12) Fernandez, A. L.; Ying Lee, T.; Reyes, C.; Prock, A.; Giering, W. P.; Haar, C. M.; Nolan, S. P. A Thermodynamic Method Based on Isoequilibrium Behavior to Determine the Values of Stereoelectronic Parameters of Phosphines. *J. Chem. Soc., Perkin Trans. 2* **1999**, No. 11, 2631–2639.

(13) Wilson, M. R.; Woska, D. C.; Prock, A.; Giering, W. P. The Quantitative Analysis of Ligand Effects (QALE). The Aryl Effect. *Organometallics* **1993**, *12* (5), 1742–1752.

(14) Woska, D.; Prock, A.; Giering, W. P. Determination of the Stereoelectronic Parameters of PF_3, PCl_3, PH_3, and $P(CH_2CH_2CN)_3$. The Quantitative Analysis of Ligand Effects (QALE). *Organometallics* **2000**, *19* (22), 4629–4638.

(15) Nelson, D. J.; Nolan, S. P. Quantifying and Understanding the Electronic Properties of N-Heterocyclic Carbenes. *Chem. Soc. Rev.* **2013**, *42* (16), 6723–6753.

(16) DiFranco, S. A.; Maciulis, N. A.; Staples, R. J.; Batrice, R. J.; Odom, A. L. Evaluation of Donor and Steric Properties of Anionic Ligands on High Valent Transition Metals. *Inorg. Chem.* **2012**, *51* (2), 1187–1200.

(17) Jarek, R. L.; Flesher, R. J.; Shin, S. K. Kinetics of Internal Rotation of N,N-Dimethylacetamide: A Spin-Saturation Transfer Experiment. *J. Chem. Educ.* **1997**, *74* (8), 978.

(18) Falivene, L.; Credendino, R.; Poater, A.; Petta, A.; Serra, L.; Oliva, R.; Scarano, V.; Cavallo, L. SambVca 2. A Web Tool for Analyzing Catalytic Pockets with Topographic Steric Maps. *Organometallics* **2016**, *35* (13), 2286–2293.

(19) Billow, B. S.; McDaniel, T. J.; Odom, A. L. Quantifying Ligand Effects in High-Oxidation-State Metal Catalysis. *Nat. Chem.* **2017**, *9* (9), 837–842.

(20) Aldrich, K. E.; Billow, B. S.; Holmes, D.; Bemowski, R. D.; Odom, A. L. Weakly Coordinating yet Ion Paired: Anion Effects on an Internal Rearrangement. *Organometallics* **2017**, *36* (7), 1227–1237.

(21) Aldrich, K. E.; Billow, B. S.; Staples, R. J.; Odom, A. L. Phosphine Interactions with High Oxidation State Metals. *Polyhedron* **2019**, *159*, 284–297.

Chapter 2. Computational Analysis of Donor Abilities of Phosphines to Vanadium(V) Nitrides

2.1 Introduction

As discussed in Chapter 1, some methods to determine the donor abilities of phosphines were discovered. Important works related to this program includes Tolman's TEP and TCA systems,[1-2] the Quantitative Analysis of Ligand Effects (QALE) method by Giering et al.,[3-5] and the cationic LDP system by Odom.[6-8]

To better understand the interaction between neutral ligands and the high valent metal center while excluding the ion-paring and solvent effects, we designed a new neutral vanadium(V) system with a similar structure as our Cr LDP system in this work (Figure 2-1).[9] By using this neutral system, we can computationally investigate high valent metal–phosphine interactions using DFT, Natural Bond Orbital theory (NBO), and Natural Resonance Theory (NRT).

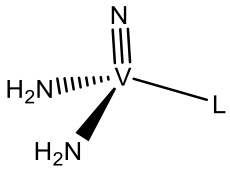

Figure 2-1. Structure of neutral vanadium(V) system studied computationally.

In previous studies, we found that metal-phosphine interactions of the Cr system have significant differences from metal-phosphine interactions of low valent metals.[7,8] With this study, we can see if these differences will be observed for vanadium(V) as well because the neutral system will be less electronegative than the cationic system. We can also analyze the resonance forms of each complex and find out how will the phosphine ligands affect the metal center. Finally, the computational barrier can be predicted to see if these values can be measured

experimentally by spin saturation NMR, and the value can be taken as a relative reference for experimental data.

This study was a collaboration with Hannah Barr. The QALE model was primarily built by Hannah. Much of the calculation work was a shared effort.

2.2 Comparison Calculation with a Late Transition Metal System

As discussed in Chapter 1, the QALE method that we want to apply to high valent metals was designed for modeling late transition metal systems.[3-5,10] To determine if the QALE method will be consistent with our expectations for a typical late transition metal reaction, we carried out a short study with a protonation reaction of nickel complexes (Scheme 2-1). The thermodynamics of this protonation of $Ni^{0}(PH_3)(PX_3)$ to $\{HNi^{II}(PH_3)(PX_3)\}^{+}$ was calculated under standard conditions using M06L functional with 6–311++G(d,p) basis set in Gaussian 16. The reaction was calculated to be exothermic and sensitive to the donor abilities of PX_3 as expected, and the two phosphines in the converged structure were held trans in all cases.

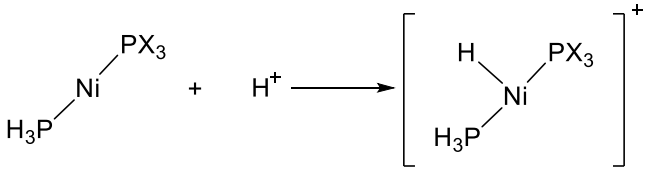

Scheme 2-1. The protonation reaction used for modeling late transition metal system.

Calculated enthalpy values of the protonation reaction in the gas phase are shown in Table 2-1.

Table 2-1. Calculated $\Delta H°$ for gas phase protonation of H_3P–Ni–PX_3.[a]

PX_3	calc. ΔH° (kcal/mol)	PX_3	calc. ΔH° (kcal/mol)
PPh_3	–247.5	$P(OMe)_3$	–231.3
$PMePh_2$	–245.3	$PHMe_2$	–230.8
PCy_3	–243.6	$P(C_6F_5)_3$	–229.4
$P(^iPr)_3$	–241.6	$P(OCH_2)_3CMe$	–226.3
PEt_3	–239.0	PH_2Me	–225.8
PMe_3	–234.6	PH_3	–220.6
PMe_2Et	–235.8	$P(CF_3)_3$	–201.5
$P(OEt)_3$	–235.5	PF_3	–197.1
PMe_2Ph	–235.2		

[a]M06L functional with 6–311++G(d,p) basis in Gaussian 16.

The reaction enthalpy was modeled by the four parameters QALE method (χ is the corrected TEP, θ denotes Tolman cone angle, E_{Ar} is the so-called aromatic effect, and π_p represents the acceptor ability of the phosphine and increases with increasing acceptor ability).

$$\Delta H°_{Ni} = a + b(\chi) + c(\theta) + d(E_{Ar}) + e(\pi_p)$$

In these regression fitting methods, we use two different methods to examine the model parameters: the natural parameter and the scaled parameter. The natural parameter is the original value one can use to calculate the expected values for a new ligand based on its QALE descriptors. The scaled parameters are scaled from the natural parameters (from –1 to +1, see *2.8 Experimental* for details), which can represent the importance of each parameter in the modeling. A larger magnitude coefficient in the scaled parameter modeling means that the parameter is more important in determining the calculated enthalpy in this case.

For this reaction, which is a late metal being protonated and oxidated from 0 to the +2 oxidation state, we can make some reasonable predictions for these four parameters. For the

σ-donor ability parameter (χ), since smaller χ means a better donor, we can predict that a smaller χ value (a more electron-rich metal center) will lead to a smaller $\Delta H°$ (more negative), which means the parameter χ and the $\Delta H°$ being modeled would go the same direction and the coefficient should be positive. We can also predict that the effect of the Tolman cone angle θ will be relatively small because the reaction only involves a proton, which has a quite small steric profile. The E_{Ar} parameter will be necessary for correcting the accuracy of some non-alkyl phosphines. For the π_p parameter, a stronger electron-withdrawing ability of the phosphine will lead to the nickel being less electron rich. In other words, a phosphine with a larger π_p will make the enthalpy of the reaction more positive.

Calculated $\Delta H°$ for gas phase protonation of H_3P–Ni–PX_3 was modeled based on the four parameters QALE method. Calculated $\Delta H°$ for gas phase protonation of H_3P–Ni–PX_3 modeled by natural parameters method is shown below:

$$\Delta H°_{Ni} = (-247 \pm 2) + (1.26 \pm 0.05)\chi + (0.01 \pm 0.01)\theta + (-6.90 + 2.86)E_{Ar} + (0.33 \pm 0.16)\pi_p$$

Calculated $\Delta H°$ for gas phase protonation of H_3P–Ni–PX_3 modeled by scaled parameters method is shown below:

$$\Delta H°_{Ni} = -230 + (24.5)\chi + (0.38)\theta + (-23.3)E_{Ar} + (3.49)\pi_p$$

The coefficient for θ was almost zero as expected. When recalculating the model without the Tolman cone angle, the same model coefficients were obtained. Both χ and π_p had a positive coefficient, which is consistent with our prediction. The electron-withdrawing ability of the phosphine plays a smaller role than the σ-donor ability of the phosphine in this reaction based on the $\Delta H°$ modeled by scaled parameters method.

This four parameter QALE method was proved to be consistent with our expectations for the late metal system. This method will be applied to the vanadium(V) nitrides system, which is an early transition metal with a high oxidation state, and investigate the difference in their metal-phosphine interactions.

2.3 Building the Vanadium(V) Nitride System

Our initial purpose for this study is to determine if it is reasonable to measure the LDP value of the target $NV(N^iPr_2)_2L$ compounds by spin saturation transfer using ^1H NMR spectroscopy. Usually, this technique requires a barrier of rotation between ~8-20 kcal/mol. We used the model system, $NV(NH_2)_2L$, to simplify the calculation. This new system was used to simulate the real process of vanadium-amide bond rotation.

The new system was initially tested to see if it can simulate the vanadium-amide bond rotation with a barrier in the ~8-20 kcal/mol range, so we tried a relatively simple B3LYP functional and cc-pVDZ basis set. The ground state of the $NV(NH_2)_2PMe_3$ complex was obtained, and the transition state of the system was found to be the structure with one of the amide groups rotated 90° (Figure 2-2).

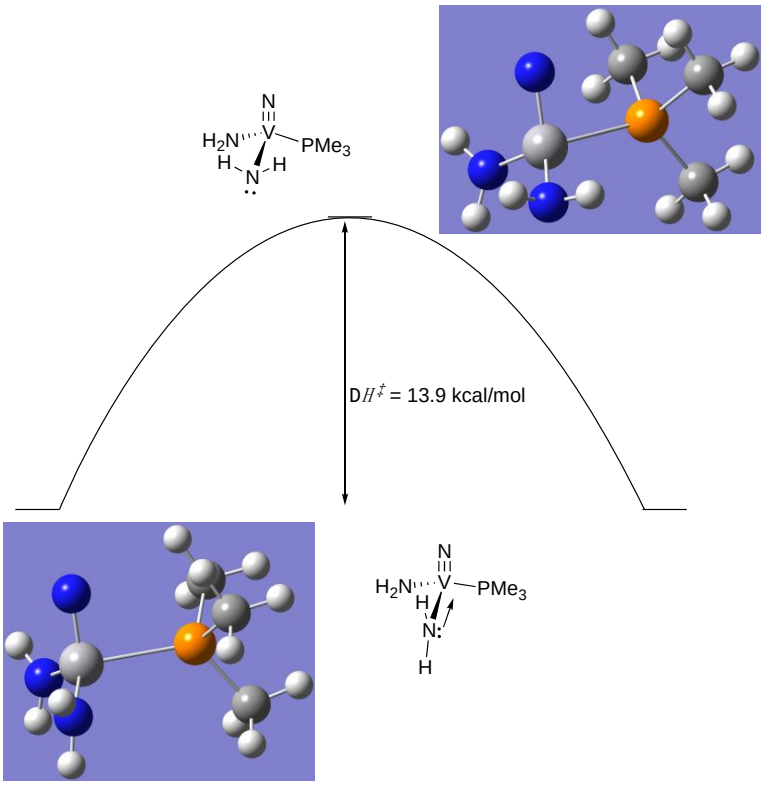

Figure 2-2. Structure of $NV(NH_2)_2(PMe_3)$ in the ground state and the transition state for amide rotation from calculations using B3LYP functional with a cc-PVDZ basis set. In the ground state, there is a strong amide lone pair donation to the metal center. In the transition state, π-bonding from the rotating amide is lost, giving pyramidal amide nitrogen.

The system successfully simulated the rotation of the vanadium-amide bond. The enthalpy differences between the ground state and the transition state were calculated and taken as LDP'_{calc} to distinguish from the previous experimental LDP values obtained for the chromium system. The LDP'_{calc} value of $NV(NH_2)_2(PMe_3)$ was 13.1 kcal/mol, which was within the range of the SST experiment requirement. Next, the LDP'_{calc} of several trialkylphosphine complexes were calculated and modeled to determine which functional and basis set would be used for further study.

2.4 Choosing the Computational Method for the Vanadium Study

After calculating $NV(NH_2)_2(PMe_3)$ with B3LYP functional and cc-PVDZ basis set, several different functionals and basis sets were chosen to calculate LDP'_{calc}. Because the LDP'_{calc}

depends heavily on the functional and basis set, it will be necessary to find an appropriate functional and basis set for further study. For this, we decided to calculate the LDP'_{calc} of several simple trialkylphosphine complexes with different functionals and basis sets. Since trialkylphosphines only have an electronic descriptor (χ) and one steric descriptor (θ) in the QALE fit, the model will be simplified. For this two descriptor QALE fit, equation of the linear regression modeling is shown below (χ is the corrected TEP, θ denotes Tolman cone angle):

$$LDP'_{calc} = a + b(\chi) + c(\theta)$$

The LDP'_{calc} of these trialkylphosphine complexes will be modeled by the equation above to give the a, b, and c values. Then one electronic parameter (χ) and one steric parameter (θ) of each trialkylphosphine will be back-calculated to give the LDP'_{model} value.

The average error between LDP'_{calc} and LDP'_{model} of each functional and basis set was calculated and given in Table 2-2.

Table 2-2. Errors for LDP'$_{calc}$ vs LDP'$_{model}$ for Various Functionals and Basis Sets.[a]

Functional	Basis Set	Average % Error	Relative Complete Time for L = P^iPr_3
B3LYP	cc-pVDZ	2.5 (0.7) [b]	1[c]
	aug-cc-pVDZ	3.9	4.9
	def2SVP	4.8	5.5
MN15	cc-pVDZ	6.4	1.7
	aug-cc-pVDZ	1.5	42
	def2SVP	2.8	8.2
M06L	cc-pVDZ	2.2 (0.2) [b]	1.5
	aug-cc-pVDZ	3.9	7
	def2SVP	4.8	4.7

[a]Average percent error between the $\Delta H^{\ddagger}$ values for ground state vs amide rotation transition for $NV(NH_2)_2L$, where L = PMe_3, PEt_3, PH_2Me, PMe_2H, PMe_2Et, P^iPr_3 found using DFT versus the model fit from experimentally derived QALE values. [b]Functional and basis set re-evaluated with a different set of ligands. L = (PMe_3, PEt_3, P^tBu_3, P^iBu_3, P^iPr_3, PCy_3). [c]This calculation required the least amount of time under the circumstances and other calculations are shown in times relative to this one under the same set of parameters (same number of nodes, etc.).

We can note that the M06L functional with cc-pVDZ basis set gave a satisfying result with only a 0.2% average error for trialkylphosphine modeling. Although the average error of MN15 functional with aug-cc-pVDZ basis set was smaller, the computational time required was significantly longer. As a result, the M06L functional with the cc-pVDZ basis set was chosen for further calculations because of its high efficiency and accuracy.

2.5 Analysis of the QALE modeling

After determining M06L functional with cc-pVDZ basis set as our final choices, we extended the calculation of *LDP'$_{calc}$* to a larger variety of phosphines, including 19 different alkyl and aryl phosphines along with phosphites. The results are shown in Table 2-3.

Table 2-3. List of PX_3 Ligands Investigated, QALE parameters,[a] and LDP'_{calc}.[b]

Ligand	χ_d	θ	E_{Ar}	π_p	LDP'calc (kcal/mol)
$P(^tBu)_3$	0	182	0	0	12.51
PCy_3	1.4	170	0	0	12.79
$P(^iPr)_3$	3.45	160	0	0	13.08
PPh_3	13.25	145	2.7	0	13.1
$P(^iBu)_3$	5.7	143	0	0	13.41
PEt_3	6.3	132	0	0	13.43
PMe_2Ph	10.6	122	1	0	13.6
$PMePh_2$	12.6	136	2.2	0	13.6
PMe_2Et	7.8	123	0	0	13.81
$P(OEt)_3$	15.8	109	1.1	2.9	13.83
PMe_3	8.55	118	0	0	13.89
$PHMe_2$	11.4	107	0	1.2	13.99
PF_3	33	104	0	13.2	14.1
$P(OCH_2)_3CH$	20.2	101	0.2	5	14.28
PH_2Me	14.4	97	0	2.5	14.31
$P(OMe)_3$	17.9	107	1	2.8	14.49
PH_3	17	87	0	3.7	14.64
$P(CF_3)_3$	33	136	0	11.1	15.29
P(C6F5)3	34.8	184	4.1	0	16.91

[a]QALE values are from the literature and the website of the originators of the method.
[b]Calculated gas-phase $\Delta H^{\ddagger}$ values for amide rotation in $NV(NH_2)_2(PX_3)$.

These *LDP'calc* values were fit based on the four parameters QALE method. As before, both natural parameters and scaled parameters were modeled. *LDP'calc* of the $NV(N^iPr_2)_2L$ system modeled by natural parameters method is shown below:

$$LDP'_{calc} = (11.9 \pm 0.1) + (0.21 \pm 0.03)\chi + (0.003 \pm 0.004)\theta + (-0.65 \pm 0.12)E_{Ar} + (-0.35 \pm 0.16)\pi_p$$

LDP'calc of the $NV(N^iPr_2)_2L$ system modeled by scaled parameters method is shown below:

$$LDP'_{calc} = 13.9 + (4.3)\chi + (0.16)\theta + (-2.26)E_{Ar} + (-3.9)\pi_p$$

For the chromium system, $\{Cr(N)(N^iPr_2)_2(PX_3)\}^+$, a previous study from our group shows that phenyl groups on phosphine ligands will increase the ligand's donor ability.[8] In this

modeling result, the coefficient of the arene parameter E_{Ar} (-2.26) means increasing numbers of aromatic groups will lower the LDP'_{calc}, which is consistent with the chromium study.

Like the nickel system we discussed before, the steric parameter θ only plays a small role in the rotation enthalpy, which makes sense since the rotation of the vanadium-amide bond only involves a very small NH_2 group. Based on the scaled parameters, the most important parameter is the σ-donor ability χ_d (4.3).

We can also note that the electron-withdrawing ability of the phosphine π_p (–3.9) is only slightly less important than χ_d. More interestingly, rather than the positive coefficient in the nickel model (0.33), the vanadium system has a negative coefficient, which means as the phosphine's π-electron withdrawing descriptor becomes larger, the LDP'_{calc} will become lower, thus the whole phosphine will become more donating toward the metal center. This phenomenon is quite counterintuitive and opposite to the result in low oxidation state late transition metals. It's also important to point out that the coefficient (–3.9) is a fairly high magnitude, hence the "electron-withdrawing" ability of the phosphine will affect the LDP'_{calc} significantly.

To explain this unusual result, Natural Bond Orbital calculations and Natural Resonance Theory analysis were carried out on a couple of representative phosphine complexes.

2.6 Resonance Structure Analysis of the Vanadium(V) Nitrides System

In the NRT analysis, to exclude the effects caused by the different conformers of each phosphine, caged phosphines were used as an example to analyze different resonance forms. To explain the reason why in a high valent metal system a phosphine with a larger electron-withdrawing parameter will lead to a larger donor ability, we compared different resonance forms of a trialkylphosphine (PR_3) and a trialkylphosphite (POR_3) complex (Figure 2-3).

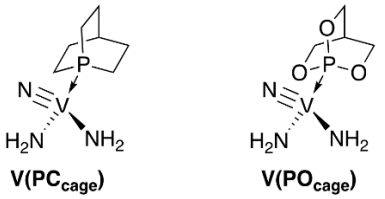

Figure 2-3. Structures of the caged trialkylphosphine and trialkylphosphite used in the NRT analysis.

The σ-donor ability will be the dominant factor for trialkylphosphines. In the trialkylphosphite complex, negative hyperconjugation will also be important. Negative hyperconjugation is the donation of electron density from a nonbonding orbital to a neighboring empty σ*-orbital.[11] In a phosphine late transition metal system, electron density usually donates from a filled *d*-orbital to an empty P–X σ*-orbital as shown in Figure 2.4. When X becomes more electronegative, negative hyperconjugation will increase due to a more stable resonance form shown on the right in Figure 2.4. For example, in the late transition metal system, this interaction will be stronger in trialkylphosphite complexes rather than trialkylphosphine complexes because the more electronegative oxygen will stabilize the negative charge.

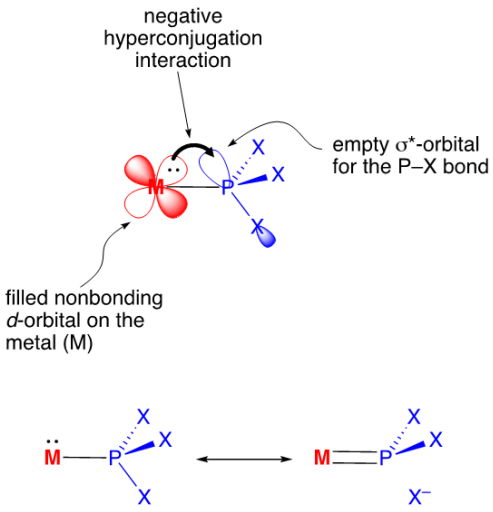

Figure 2-4. Examples of negative hyperconjugation in a late transition metal system, where the electron density donates from a filled *d*-orbital to an empty P–X σ*-orbital. As X becomes more electronegative, the more stable resonance form will lead to a stronger interaction.

In a high oxidation state early transition metal system like vanadium(V) or chromium(VI), due to the d^0 electron shell structure, negative hyperconjugation cannot occur from the metal. But the calculations for the vanadium and chromium systems previously published[8] show that the electron-withdrawing parameter π_p plays a significant role in increasing the electron density of the metal.

The resonance forms of a trialkylphosphine system V(PC_{cage}) are shown in Figure 2.5. The major contributed resonance form (57%) is the one where the phosphorus donates its lone pair to vanadium, placing a negative charge on the metal center and a positive charge on phosphorus. This form is labeled as α. In the second contributed resonance form β (37%), the lone pair electron remains on phosphorus and there is no bond between vanadium and phosphine. The α and β resonance forms contribute 94% of the NRT description. The remaining 6% due to the Lγ form is a structure where a filled orbital on vanadium (the vanadium-nitride bonding orbital) donates into the P–C antibonding orbitals. This form is similar to the negative hyperconjugation

interaction in the late transition metal system in Figure 2-4, but the electron density is donated from a bonding orbital instead of a nonbonding orbital.

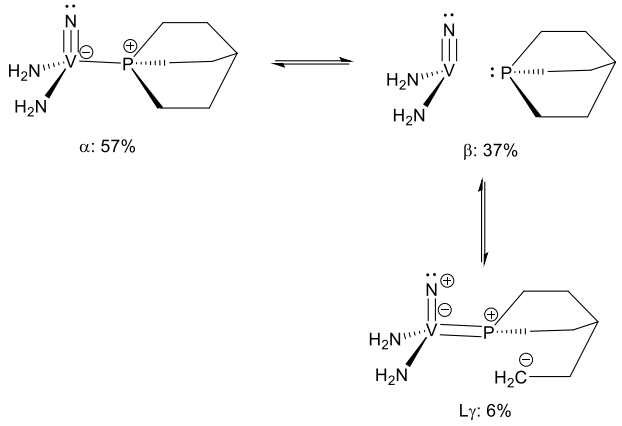

Figure 2-5. Natural Resonance Theory analysis of V(PC_{cage}) under M06L/cc-pVDZ and NBO7.

The resonance forms of the trialkylphosphite system V(PO_{cage}) are shown in Figure 2-6. Due to the oxygens having higher electronegativity, the α form only contributes 32% to the NRT description. But in the trialkylphosphite system, a new hyperconjugative form (Xγ) was observed. In this largest contributor (42%), lone pair electron density on one oxygen donates into the P–O antibonding orbital of another oxygen on phosphorus and the V–P bond is retained. With the help of this Xγ resonance form, the sum of forms with a V–P single bond accounts for 74%, resulting in a relatively small contribution from β (24%).

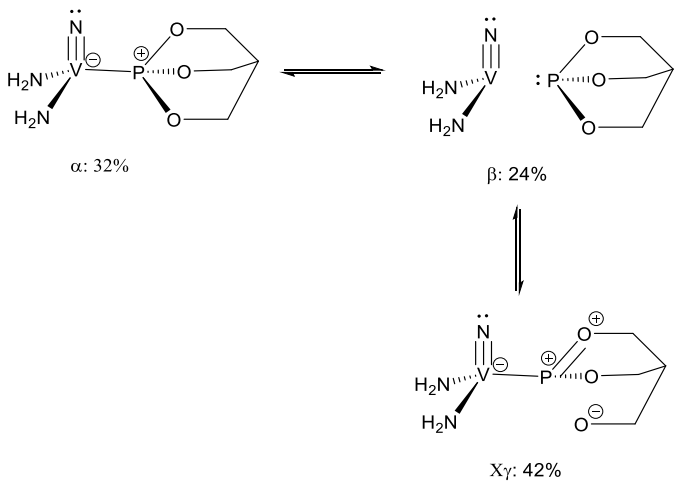

Figure 2-6. Natural Resonance Theory analysis of V(PO_{cage}) under M06L/cc-pVDZ and NBO7. There is a 2% contribution from additional minor forms not shown.

Studies for known d^0 early transition metal systems where both phosphites and phosphines were reported are relatively rare. In M. L. H. Green and coworker's study,[12] the niobium(V) phosphite complex Nb(=$NNMe_2$)(Cp)Cl_2{$P(OMe)_3$} was reported with a Nb–P distance of 2.6030(6) Å. An almost identical system,[13] Nb(=NMe)(Cp)Cl_2(PMe_3), reported by V. C. Gipson showed an Nb–P distance of 2.604(2) Å, which is identical to the phosphite system (Figure 2-7).

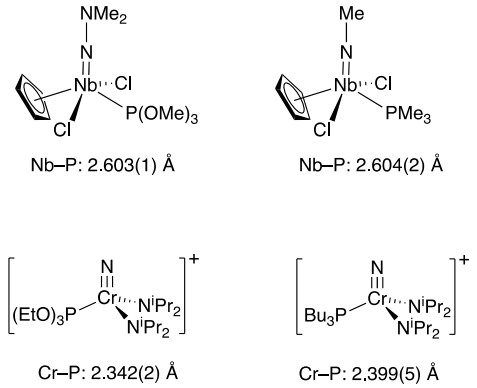

Figure 2-7. Comparisons of M–P bond distances in similar d^0 phosphite and phosphine systems. Bond distances from X-ray diffraction.

According to the computational converged ground state structures of V(PC_{cage}) and V(PO_{cage}) complexes, the calculated V–P bond distance of the V(PC_{cage}) complex is 2.468(4) Å

and 2.449(7) Å for V(PO_{cage}) complex, in which the distance in phosphite complex is shorter than the phosphine complex. For comparison, two examples from the previous study are shown in Figure 2-7.[8] In this case, the phosphite complex also shows a significantly shorter Cr–P bond distance than the phosphine one. This difference can be due to Xγ contributions like in Figure 2-6.

When comparing LDP'_{calc} of PO_{cage} and PC_{cage}, we can note that PO_{cage} has a LDP'_{calc} value (14.28 kcal/mol) larger than PC_{cage} (13.85 kcal/mol), suggesting that V(PO_{cage}) is a weaker Lewis base. But the calculated V–P bond orders in V(PC_{cage}) and V(PO_{cage}) are very similar at 0.67 and 0.71, respectively. Both V–P bond orders and natural bond orbital analysis are consistent with our assumption that there are significant differences in how the two types of ligands interact with the metal center and the resonance forms participating.

2.7 Concluding Remarks

In this study, we designed a new calculated system, the $NV(NH_2)_2(PX_3)$ complex, to determine if a type of neutral vanadium nitride complexes $NV(NR_2)_2(PR_3)$ will have barriers to amide rotation in a typical range for the spin saturation transfer measurement. We also did NBO and NRT analysis to explore how phosphine ligands interact with the metal center and how they affect the barriers to amide rotation.

After calculating the enthalpic barrier (LDP'_{calc}) to the rotation of 19 different $NV(NH_2)_2(PX_3)$ complexes, we found that all their LDP'_{calc} values are in the ~12-17 kcal/mol range, which is well situated for the experimental donor ability measurement. We also did the four parameters QALE model for the LDP'_{calc} values. The modeling results suggests that trialkylphosphines and trialkylphosphites may have similar donor abilities. By comparing QALE descriptors in an early transition metal system and a late transition metal system, we noticed that

in the vanadium nitride system, the π-electron withdrawing descriptor (*e* coefficient on π_p) has a similar magnitude to the σ-donor ability descriptor (*a* coefficient on χ), leading to an increased donation in late transition metal systems.

From NRT analysis, this difference can be explained by the negative hyperconjugation between the phosphite ligand (Xγ resonance form in Figure 2-6) and the metal. In this form, the negative hyperconjugation is not from the metal to ligand orbitals, but one oxygen to the P–O antibonding orbital of another oxygen. With the help of this Xγ resonance form, the contributions of resonance forms with V–P bonds in the trialkylphosphine and trialkyl phosphites are similar.

This result suggests that in high oxidation state metal complexes, phosphites and phosphines may have a similar donor ability. Xγ resonance form may overcome the σ-electron withdrawing effects of oxygens and plays an important role in the overall donor abilities of phosphites.

2.8 Experimental

Experimental taken from recent publication: This can be located at:

Mo, L.; Barr, H. I.; Odom, A. L. *Results in Chemistry* **2022**, *4* (100344), 100344, DOI:10.1016/j.rechem.2022.100344.

Instrumentation and Facilities. All calculations were carried out at the High-Performance Computing Center (HPCC) through Michigan State University's Institute for Cyber-Enabled Research. DFT optimizations were performed using Gaussian16 and the Natural Bond Orbital (NBO) program *NBO 7.0* for all vanadium compounds.

Modeling Approach. The fits were done using both the "natural" variables, the direct QALE values and LDP', and scaled variables. The natural variables give a model that can be used to calculate the LDP' of the ligands to predict new LDP'. The scaled variables allow direct comparison between the different parameters and comparison of various QALE factors. The scaling was done using the equation below, where x_i= scaled variable, u_i= natural variable, u_i^0= midpoint of the range of the natural variables, and Δu_i= the difference between the midpoint and the high value (~half the full range).

$$X_i = \frac{u_i - u_i^0}{\Delta u_i}$$

The equations for the calculation of u_i^0 and Δu_i are shown below.

$$\Delta u_i = u_i^{high} - u_i^0$$

$$u_i^0 = \frac{u_i^{high} + u_i^{low}}{2}$$

Using either the scaled or natural variables, a least squares fit to the data was done by solving the equation below, sometimes called the "Normal Equation". In the equation, y = vector of the enthalpies to be fit, b = single column matrix of the parameters (i.e., *a, b, c, d,* and *e* in the manuscript), X = the model matrix which consists of the scaled or unscaled descriptor values. The equation below provides the least square values without being prone to local minima like iterative methods can be and required nothing more than an Excel spreadsheet to calculate the set of coefficients, although other programs that can carry out linear algebra operations can be used to obtain the fit.

$$(X^t \cdot X)^{-1} \cdot X^t \cdot y = b$$

To get the a-coefficient in the fit, a row of ones was added before the QALE data. Solution of the above equation gives a = 11.8, b = 0.21, and c = 0.003, d = -0.65, e =

-0.35. The scaled variable coefficients were found similarly.[14]

Error Analysis of Model Coefficients. For each coefficient in the model, the error was calculated by rearranging the model equation to solve for a list of the optimized coefficients for each ligand, then calculating Student's t-distribution.[15] First, the model equation was rearranged and set to equal the coefficient in question. The general form of the model is represented in Eq. 1, and an example of the rearrangement to solve for coefficient b is represented in Eq. 2. Then, the optimized coefficient b was solved for each ligand. Holding the rest of the model constant while solving for an optimized coefficient for each ligand allows a spread of data that can be analyzed to see how accurately the model coefficient represents the optimized coefficients.

$$LDP' = a + b(\mathrm{X}) + c(\varepsilon) + d(\pi) + e(E_{ar}) \quad (1)$$

$$b = \frac{LDP' - a - c(\varepsilon) - d(\pi) - e(E_{ar})}{\chi} \quad (2)$$

To determine the error value, first the average was tabulated. Each calculated value was then subtracted from the mean, squared, then summed. The quantity was then divided by the square root of $N - 1$, N = number of values in the set (Eq. 3). This number was then divided by the square root of N and multiplied by $t_{0.99}$ from a *Critical value of t*[a] table (Eq. 4).[14]

$$S = \frac{1}{\sqrt{N-1}} [\sum_{i=1}^{N} (x_i - \bar{x})^2]^{1/2} \quad (3)$$

$$\Delta = t_{0.99} \frac{S}{\sqrt{N}} \quad (4)$$

Table 2-4. QALE Values for Phosphines in Nickel Study.

Ligand	Intercept	X	θ	E(ar)	π(p)
PMe_3	1	8.55	118	0	0
PEt_3	1	6.3	132	0	0
P^iPr_3	1	3.45	160	0	0
PMe_2Ph	1	10.6	122	1	0
PH_3	1	17	87	0	3.7
$P(OMe)_3$	1	17.9	107	1	2.8
$P(OEt)_3$	1	15.8	109	1.1	2.9
$PMePh_2$	1	12.6	136	2.2	0
PF_3	1	33	104	0	13.2
$P(CF_3)_3$	1	33	136	0	11.1
PCy_3	1	1.4	170	0	0
$P(OCH_2)_3CH$	1	20.2	101	0.2	5
PH_2Me	1	14.4	97	0	2.5
$PHMe_2$	1	11.4	107	0	1.2
PMe_2Et	1	7.8	123	0	0
$P(C_6F_5)_3$	1	34.8	184	4.1	0
PPh_3	1	13.25	145	2.7	0

REFERENCES

(1) Tolman, C. A. Steric Effects of Phosphorus Ligands in Organometallic Chemistry and Homogeneous Catalysis. *Chem. Rev.* **1977**, *77* (3), 313–348.

(2) Tolman, C. A. Electron Donor-Acceptor Properties of Phosphorus Ligands. Substituent Additivity. *J. Am. Chem. Soc.* **1970**, *92* (10), 2953–2956.

(3) Rahman, M. M.; Liu, H. Y.; Prock, A.; Giering, W. P. Quantitative Analysis of Ligand Effects. 2. Steric and Electronic Factors Influencing Transition-Metal-Phosphorus(III) Bonding. *Organometallics* **1987**, *6* (3), 650–658.

(4) Wilson, M. R.; Woska, D. C.; Prock, A.; Giering, W. P. The Quantitative Analysis of Ligand Effects (QALE). The Aryl Effect. *Organometallics* **1993**, *12* (5), 1742–1752.

(5) Fernandez, A. L.; Reyes, C.; Prock, A.; Giering, W. P. The Stereoelectronic Parameters of Phosphites. The Quantitative Analysis of Ligand Effects (QALE). *J. Chem. Soc., Perkin Trans. 2* **2000**, No. 5, 1033–1041.

(6) DiFranco, S. A.; Maciulis, N. A.; Staples, R. J.; Batrice, R. J.; Odom, A. L. Evaluation of Donor and Steric Properties of Anionic Ligands on High Valent Transition Metals. *Inorg. Chem.* **2012**, *51* (2), 1187–1200.

(7) Aldrich, K. E.; Billow, B. S.; Holmes, D.; Bemowski, R. D.; Odom, A. L. Weakly Coordinating yet Ion Paired: Anion Effects on an Internal Rearrangement. *Organometallics* **2017**, *36* (7), 1227–1237.

(8) Aldrich, K. E.; Billow, B. S.; Staples, R. J.; Odom, A. L. Phosphine Interactions with High Oxidation State Metals. *Polyhedron* **2019**, *159*, 284–297.

(9) Mo, L.; Barr, H. I.; Odom, A. L. Investigation of Phosphine Donor Properties to Vanadium(V) Nitrides. *Results in Chemistry* **2022**, *4* (100344), 100344.

(10) Kühl, O. Predicting the net donating ability of phosphines-do we need sophisticated theoretical methods? *Coord. Chem. Rev.* **2005**, *249* (5–6), 693–704.

(11) McNaught, A.; Wilkinson, A. *Compendium of chemical terminology (Vol. 1669)*; Blackwell Science: Oxford, 1997.

(12) Green, M. L. H.; Thomas James, J.; Saunders, J. F.; Souter, J. Half-Sandwich Hydrazido(2−) Complexes of Niobium. *J. Chem. Soc., Dalton Trans.* **1997**, No. 8, 1281–1288.

(13) Williams, D. N.; Mitchell, J. P.; Poole, A. D.; Siemeling, U.; Clegg, W.; Hockless, D. C. R.; O'Neil, P. A.; Gibson, V. C. Half-Sandwich Imido Complexes of Niobium and Tantalum. *J. Chem. Soc., Dalton Trans.* **1992**, No. 5, 739.

(14) Carlson, R.; Carlson, J. E. *Design and Optimization in Organic Synthesis*; Elsevier Science: London, England, 2005.

(15) Shoemaker, D. P.; Nibler, J. W. *Experiments in Physical Chemistry 5th Ed*; McGraw-Hill: New York, 1989.

Chapter 3. Experimental Studies of Donor Abilities of Neutral Ligands to Vanadium(V) Nitrides

3.1 Introduction

As discussed in Chapter 1 and Chapter 2, the experimental target complex will be $N{\equiv}V(NR_2)_2L$ (L=a neutral ligand), which has a similar structure as our Cr LDP system. However, examples of terminal vanadium(V) nitrido complexes are rare due to decomposition during ligand replacement and infrequent sources of molecular precursors. Actually, for V(III) and V(IV), vanadium nitrido complexes are still unknown. And there are only a few examples of neutral vanadium(V) nitrido complexes.[1-4] So far, the only characterized neutral vanadium(V) nitrido complexes with neutral ligands were reported by Nancy M. Doherty and coworkers, in which they used pyridine and quinuclidine donors to stabilize the complex.[2] In Doherty's work, $Cl_3V{\equiv}NSiMe_3$, a volatile and temperature sensitive complex, was used as the precursor.

More common examples of vanadium(V) nitrides are anionic.[5-8] In these studies, $VCl(NR_2)_2$ or $V(NR_2)_3$ was prepared from $VCl_3(THF)_3$ by reacting with 2 or 3 equivalents of $LiNR_2$. Then, an azide source was used to oxidize the precursor to the target anionic vanadium(V) nitride complex. An interesting fact is that all these complexes above must contain one or two aromatic groups in the amides. One possible explanation is that β-hydride elimination can occur during halide replacement, which is prevented by having aromatic groups. In these studies, Farrell and Bukhryakov suggest that although both bimolecular decomposition and β-hydride elimination contribute to the decomposition of vanadium(V) imido complexes, the major pathway is β-hydride elimination. [9-11]

In this Chapter, I will delineate the synthesis and characterization of some new vanadium(V) imido complexes, along with new synthetic methods and characterization of

prepared vanadium(V) nitrido complexes. Also, LDP measurements were carried out for some neutral ligands attached vanadium(V) imido complexes.

3.2 Synthesis and Characterization

Since Doherty's work[2] provided the only known vanadium(V) nitrido complexes with neutral ligands attached, the precursor she used, $Cl_3V{\equiv}NSiMe_3$, was taken as our starting material. The starting material $Me_3SiN{=}V(OSiMe_3)_3$ (**1**) was prepared on large scales from NH_4VO_3 and excess $HN[Si(CH_3)_3]_2$.[13] The product is a light-yellow solid purified by vacuum distillation over 137 °C.

After following the Doherty procedure, which is a metathesis reaction between $(Me_3SiO)_3V{=}NSiMe_3$ and $VOCl_3$ followed by sublimation, it was found that the product $Cl_3V{\equiv}NSiMe_3$ is volatile and metastable at room temperature, decomposition occurred during purification. Matthias's group used $TiCl_4$ as the Cl source and reported a higher yield of the $(Me_3SiO)_3V{=}NSiMe_3$ product.[12] They also used vacuum sublimation to purify the crude product. Although the yield might be higher using $TiCl_4$, the impurities carried forward during sublimation were not acceptable for further synthesis. In this work, $Me_3SiN{\equiv}VCl_3$ (**2**) was directly synthesized from $Me_3SiN{=}V(OSiMe_3)_3$ and $TiCl_4$, and purified by multiple recrystallizations from pentane, which was much easier to carry out and gave a reasonable yield of 52% (Scheme 3-1). Orange needle-shaped crystals of **2** are volatile and temperature sensitive, which will decompose in 2 hours at room temperature.

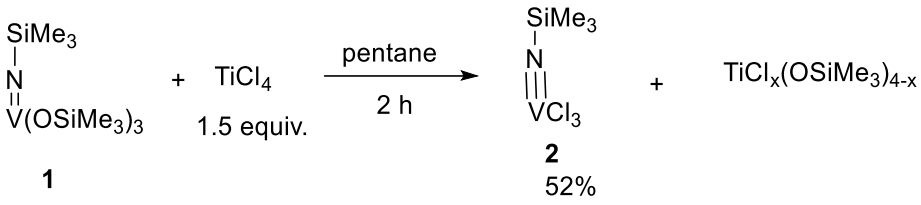

Scheme 3-1. Synthesis of $Cl_3V{\equiv}NSiMe_3$ (**2**).

Compound **2** was then treated with a series of neutral ligands. Pyridine (py) was first tried based on the previous study,[2] but the product, $[N{\equiv}VCl_2(py)_2]_\infty$, was a brick-red polymer that was insoluble in any solvent.

By changing pyridine to 4-*tert*-butylpyridine, $N{\equiv}VCl_2(4\text{-}t\text{-bupy})_2$ was successfully obtained and characterized by X-ray diffraction and NMR spectroscopy (Scheme 3-2). Compound **3** was purified by recrystallization from toluene/pentane. Red crystals of **3** are stable at room temperature and will decompose on exposure to dichloromethane (Figure 3-1).

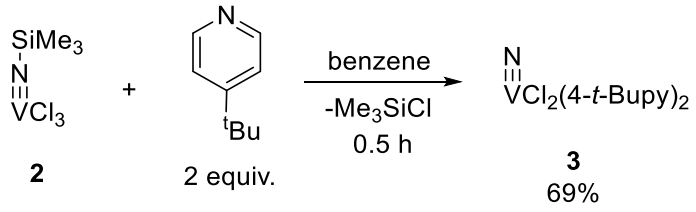

Scheme 3-2. Synthesis of $N{\equiv}VCl_2(4\text{-}t\text{-bupy})_2$ (**3**).

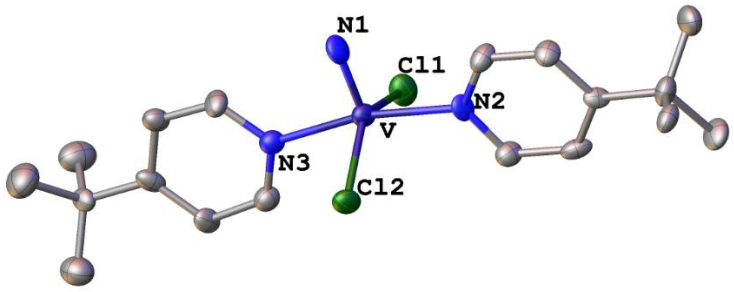

Figure 3-1. Structure of **3** from X-ray Diffraction. Ellipsoids displayed at the 50% probability level. All hydrogens in the lattice were removed for clarity.

The X-ray structural study proves Doherty's hypothesis that **3** is monomeric in the solid state. Similar to $N{\equiv}VCl_2(quin)_2$, ligands around the vanadium center define a distorted trigonal bipyramidal geometry.[2] The V-N1 bond distance of 1.58(2) Å is shorter than V-N2 (2.095(18) Å) and V-N3 (2.151(19) Å), suggesting a strong vanadium-nitrogen triple bond (Table 3-1).

Table 3-1. Selected Bond Distances (Å) and Angles (deg) for $N{\equiv}VCl_2(4\text{-}t\text{-bupy})_2$ (**3**).

	3
V-N1	1.58(2)
V-N2	2.151(19)
V-N3	2.095(18)
V-Cl1	2.246(7)
V-Cl2	2.284(8)
N1-V-N2	94.7(9)
N1-V-N3	95.9(9)
N2-V-N3	169.2(8)
Cl1-V-Cl2	140.8(3)
Cl1-V-N1	109.4(7)
Cl2-V-N1	109.8(7)
Cl1-V-N2	87.3(7)
Cl2-V-N2	88.6(7)
Cl1-V-N3	87.4(7)
Cl2-V-N3	89.6(7)

Complex **3** was then reacted separately with 2 equivalents of lithium diisopropylamide, lithium diethylamide and lithium dimethylamide. All three reactions led to a black sticky oil. The ^{1}H NMR of these crude oils only showed free 4-*tert*-butylpyridine and messy peaks, suggesting that decomposition occurred in these reactions. No characterized product can be isolated from these sticky oils. Reactions between $Me_3SiN{\equiv}VCl_3$ (**2**) and 1, 2 or 3 equivalents of lithium diisopropylamide also led to decomposition.

In 2008, Bart Hessen and co-workers reported the reaction of p-tol$N{=}VCl_3$ with 2 equivalents of diisopropylamine.[14] A similar reaction works well with $Me_3SiN{=}VCl_3$ (**2**).

Scheme 3-3 summarizes the reaction of $Me_3SiN{\equiv}VCl_3$ (**2**) with excess diisopropylamine to give $Me_3SiN{=}VCl_2(N^iPr_2)$ (**4**) in 71% isolated yield.

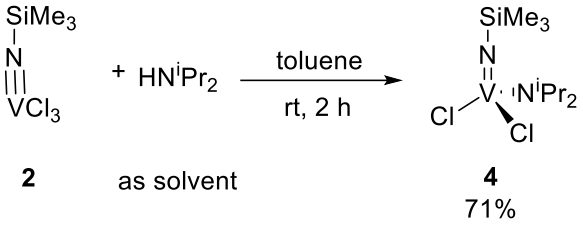

Scheme 3-3. Synthesis of $Me_3SiN{=}VCl_2(N^iPr_2)$ (**4**).

To ensure complete formation of **4**, **2** was dissolved in toluene, and excess equivalents of diisopropylamine were added. After stirring at room temperature for 2 h, all volatiles were removed. The resulting dark red solid was extracted with pentene and stored at -30 ℃ overnight, affording red crystals (Figure 3-2) of **4** in 71% isolated yield. In the starting material **2**, the nitrogen-vanadium bond was usually taken as a triple bond because the bond length of it (1.59(1) Å)[15] is close to the neutral monomeric vanadium nitride bond (1.568(19) Å in $N{\equiv}VCl_2(quin)_2$).[2] Surprisingly, single crystal X-ray diffraction (XRD) studies of **4** (Table 3-2) showed the molecular connectivity featuring a mononuclear pseudotetrahedral vanadium center having a longer V=N1 bond distance of 1.634(6) Å, similar to the known V=N form (1.666(2) Å in $CpV(N\text{-}p\text{-}tol)(N^iPr_2)Me$).[14] The V-N1 amide bond (1.810(6) Å) was consistent with the bond length of the V-N single bond published before (1.851(2) Å in $CpV(N\text{-}p\text{-}tol)(N^iPr_2)Me$).[14]

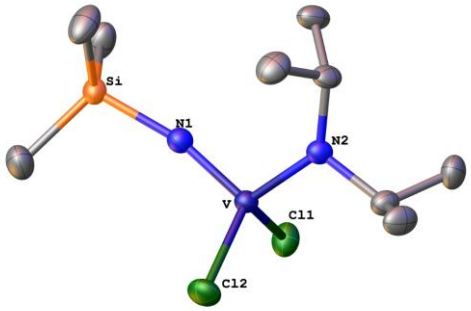

Figure 3-2. Structure of **4** from X-ray Diffraction. Ellipsoids displayed at the 50% probability level. All hydrogens in the lattice were removed for clarity.

Table 3-2. Selected Bond Distances (Å) and Angles (deg) for $Me_3SiN{=}VCl_2(N^iPr_2)$ (**4**).

	4
V-N1	1.634(6)
V-N2	1.810(6)
V-Cl1	2.224(2)
V-Cl2	2.216(2)
N1-Si	1.771(6)
N1-V-N2	104.7(3)
N1-V-Cl1	109.5(2)
N1-V-Cl2	108.5(2)
Si-N1-V	167.0(4)
N2-V-Cl1	110.86(18)
N2V-Cl2	108.63(18)
Cl1-V-Cl2	114.22(8)

Compound **4** was also reacted with 1 or 2 equivalents of lithium diisopropylamide in THF in an attempt to form $Me_3SiN{=}VCl(N^iPr_2)_2$ or $Me_3SiN{=}V(N^iPr_2)_3$, but both reactions gave a messy ^1H NMR spectrum. No characterizable product was isolated from the resulting dark solution.

Scheme 3-4 shows the general synthesis of **4-L** from **4** and neutral ligands. Most of the **4-L** products were achieved by adding neutral ligands' pentane solution dropwise to **4**. The resulting solution was then concentrated, and crystals of **4-L** were obtained after 12 h at -30 °C. Due to the poor solubility of 4-dimethylaminopyridine (DMAP) in pentane, reaction of **4** and DMAP

was in chloroform and the crystals were obtained from layered chloroform and pentane. For all of these neutral ligands, more than one equivalent of ligands will give the same result as one equivalent. P^iPr_3, PPh_3, and P^tBu_3 were also tried with the same procedure, but only PMe_3 reacted with **4**. By ^1H NMR spectroscopy, P^iPr_3, PPh_3, and P^tBu_3 will remain free in solutions of **4**.

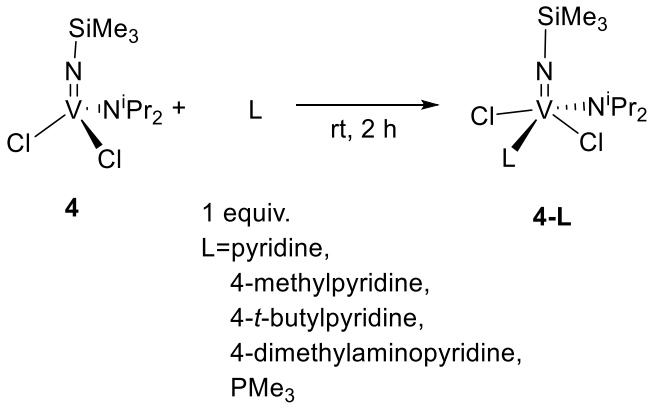

Scheme 3-4. General synthesis of $Me_3SiN{=}VCl(N^iPr_2)_2L$ (**4-L**), L= pyridine, 4-methylpyridine, 4-*tert*-butylpyridine, 4-dimethylaminopyridine, trimethylphosphine.

XRD studies were carried out for **4-Py**, **4-Mepy**, **4-DMAP** and **4-PMe3** (Figure 3-3). All of these structures show a pseudo-square pyramidal vanadium center (geometry index τ_5: **4-Py** 0.156, **4-Mepy** 0.157, **4-DMAP** 0.051, **4-PMe3** 0.340) with a V=N distance similar to **4** (Table 3-3). Unlike **4-Py**, **4-Mepy** and **4-PMe3**, the two Cl in **4-DMAP** structure are not opposite to each other on the square plane, which leads to a relatively smaller geometry index τ_5 value.

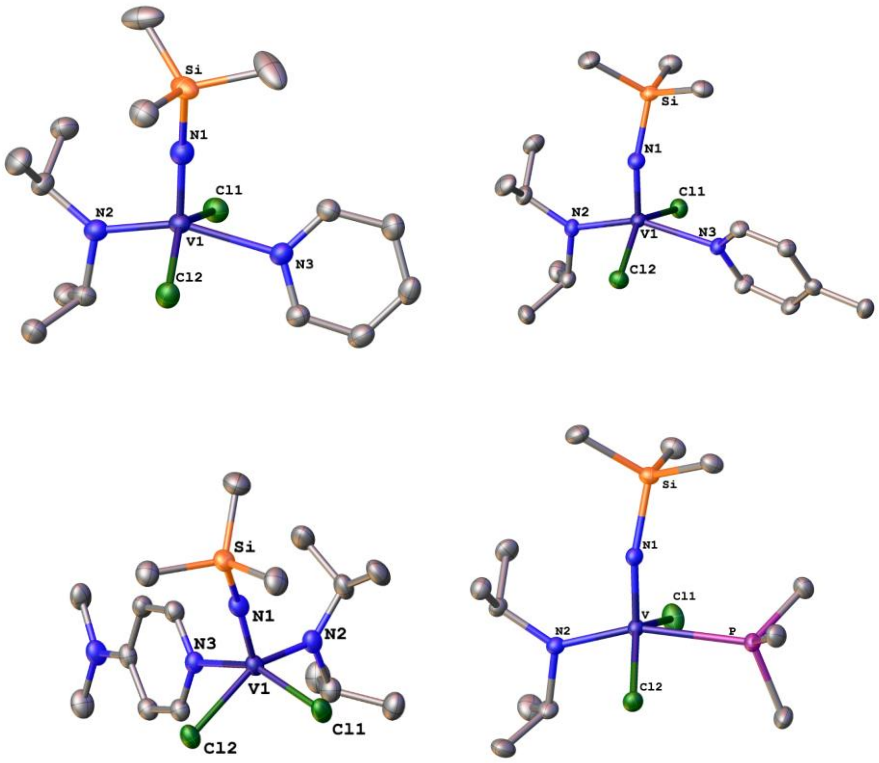

Figure 3-3. Structure of **4-Py**, **4-Mepy**, **4-DMAP** and **4-PMe$_3$** from X-ray Diffraction. Ellipsoids displayed at the 50% probability level. All hydrogens and solvent (chloroform in **4-DMAP**) in the lattice were removed for clarity.

Table 3-3. Selected Bond Distances (Å) and Angles (deg) for **4-Py**, **4-Mepy**, **4-DMAP** and **4-PMe3**.

	4-Py	**4-Mepy**	**4-DMAP**	**4-PMe3**
V-N1	1.632(3)	1.635(2)	1.635(2)	1.645(2)
V-N2	1.849(3)	1.843(2)	1.844(2)	1.852(2)
V-Cl1	2.3496(10)	2.3142(8)	2.3691(6)	2.3107(8)
V-Cl2	2.3266(10)	2.3458(8)	2.3809(6)	2.3332(7)
V-N3	2.219(3)	2.213(2)	2.1252(19)	-
V-P	-	-	-	2.5516(8)
N1-Si	1.771(3)	1.772(3)	1.768(2)	1.766(2)
V-N1-Si	164.8(2)	160.83(16)	157.64(13)	159.32(15)
N1-V-N2	103.59(14)	103.40(11)	90.25(8)	106.44(10)
Cl1-V-Cl2	145.47(4)	145.65(3)	83.62(2)	139.05(3)
Cl1-V-N1	106.66(11)	104.21(9)	102.76(7)	105.82(8)
Cl2-V-N1	104.96(11)	107.28(9)	105.86(7)	110.93(8)
Cl1-V-N2	90.73(9)	94.04(8)	91.73(6)	93.39(7)
Cl2-V-N2	95.07(9)	91.76(8)	151.67(7)	93.05(7)
N1-V-N3	101.30(13)	101.43(11)	101.36(9)	-
N2-V-N3	154.83(12)	155.05(10)	90.25(8)	-
Cl1-V-N3	78.53(8)	82.16(7)	154.76(6)	-
Cl2-V-N3	82.04(8)	78.53(7)	82.77(5)	-
N1-V-P	-	-	-	94.10(8)
N2-V-P	-	-	-	159.46(7)
Cl1-V-P	-	-	-	80.49(3)
Cl2-V-P	-	-	-	79.51(3)

Since the expected Me_3SiCl elimination (similar to the reaction from **2** to **3**) did not occur when **4** was reacted with neutral ligands, several Me_3SiCl eliminating methods were attempted on **4-Py**. Complex **4-Py** remained stable after refluxing in toluene overnight. Some tetrafluoroborate salts (including $NaBF_4$, $AgBF_4$ and $[HPy]^+ BF_4^-$) and some fluoride salts (including SnF_2 and KF (18-crown-6)) were reacted with **4-Py**, but all these reactions led to mixtures that could not be characterized.

Sandro Gambarotta and coworkers reported the reaction of a base like LiHN^{i}Pr or LiMe to eliminate the trimethylsilyl group from $Me_3SiN=V(NPh_2)_3$.[5] Since a strong base like LiN^{i}Pr$_2$ will lead to decomposition of **4**, a weaker base $KOSiPh_3$ was selected.

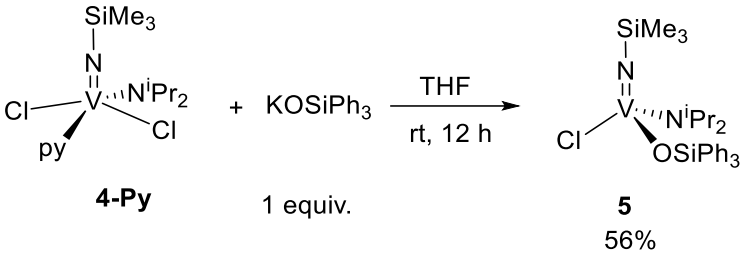

Scheme 3-5. Synthesis of $Me_3SiN=VCl(N^{i}Pr_2)(OSiMe_3)$ (**5**).

Scheme 3-5 shows the formation of $Me_3SiN=VCl(N^{i}Pr_2)(OSiMe_3)$ (**5**) from **4-Py** and $KOSiPh_3$. Rather than eliminating Me_3SiCl and forming $Me_3SiOSiPh_3$, KCl and $N{\equiv}VCl(py)(N^{i}Pr_2)$, one of the Cl groups in **4-Py** was replaced by the $OSiPh_3$ group and the pyridine released as a free pyridine. Crystals of **5** were obtained from layered toluene and pentane. An XRD study of **5** is shown in Figure 3-4.

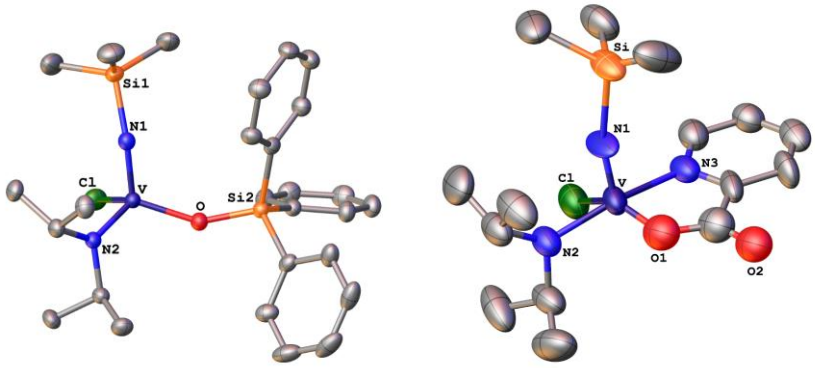

Figure 3-4. Structure of **5** and **6** from X-ray Diffraction. Ellipsoids displayed at the 50% probability level. All hydrogens in the lattice were removed for clarity.

Another synthetic approach towards vanadium nitride was from **4-Py** and another base potassium pyridine-2-carboxylate (Scheme 3-6). As **5**, one of the Cl groups in **4-Py** was replaced

and formed $Me_3SiN=VCl(N^iPr_2)$(pyridine-2-carboxylate) (**6**). Crystals of **6** were obtained from layered toluene and pentane and studied by single crystal X-ray diffraction (Figure 3-4).

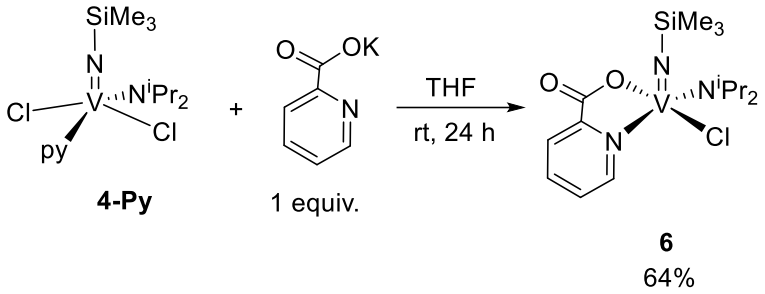

Scheme 3-6. Synthesis of $Me_3SiN=VCl(N^iPr_2)$(pyridine-2-carboxylate) (**6**).

6 was then stirred in toluene under 100°C for 24 h. The TMS group was expected to be eliminated with a 6-membered cyclic transition state (Scheme 3-7). But after heating, only black precipitates which cannot dissolve in toluene were gotten, suggesting the decomposition of **6**. The same reaction condition with the presence of excess equivalents of pyridine was repeated for **6**, resulting the same undissolvable black solid.

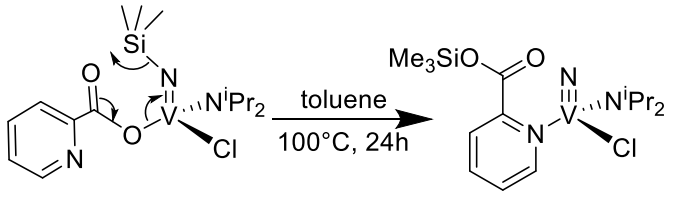

Scheme 3-7. Expected TMS elimination under high temperature from **6**.

3.3 Ligand Donor Ability (LDP) Determination

As discussed in Chapter 1, in the Cr system, to measure LDP, the rotation rate of the amide will be measured using ^1H NMR spin saturation transfer. Then, the Eyring equation will be used to convert this rotation rate to the $\Delta G^{\ddagger}$ value. Under the assumption that $\Delta S^{\ddagger}$ = -9 e.u., the temperature independent enthalpic barrier to the rotation, $\Delta H^{\ddagger}$, is taken as LDP (kcal/mol).[16]

In this study, LDP values of **4**, **4-Py**, **4-Mepy**, **4-^{t}bupy**, **4-DMAP** and **4-PMe$_3$** were measured (Table 3-3). All complexes gave a relatively high $\Delta H^{\ddagger}$ value and a positive $\Delta S^{\ddagger}$ value. Also, the values for the entropies were found to vary widely.

Table 3-4. Measured $\Delta H^{\ddagger}$ and $\Delta S^{\ddagger}$ values of **4**, **4-Py**, **4-Mepy**, **4-^{t}bupy**, **4-DMAP** and **4-PMe$_3$** from Eyring plots.

Complex	$\Delta H^{\ddagger}$ (kcal/mol)	$\Delta S^{\ddagger}$ (e.u.)
4	19.79±0.38	3.71±1.21
4-Py	20.71±0.27	6.04±0.86
4-Mepy	22.99±0.61	13.03±1.98
4-tbupy	23.42±0.19	14.33±0.61
4-DMAP	22.34±0.90	9.19±2.90
4-PMe$_3$	26.57±0.57	23.79±1.84

Unlike the previous chromium nitride LDP system, this vanadium imido system retain a large trimethylsilyl group on the nitrogen atom. When the amide rotates, the trimethylsilyl group may obstruct rotation, leading to these positive $\Delta S^{\ddagger}$ values.

3.4 Conclusion Remarks

In this work, several new vanadium imido complexes were synthesized and characterized. Regrettably, the resulting vanadium imido complexes were not suitable for the desired LDP measurement, and attempts to eliminate the trimethylsilyl group forming vanadium nitride complexes were not generally successful.

As discussed before, a more commonly used synthetic route for vanadium nitrido complexes is to graft anionic nitrides onto vanadium. [5-8] By following Gambarotta's procedure, an ionic vanadium nitride complex $[Li(THF)_{3.5}]^+[N{\equiv}V(Ph_2N)_3]^-$ was obtained. Studies of synthesizing neutral vanadium nitride complexes from this product are ongoing.

3.5 Experimental

General Considerations. All reactions and manipulations were carried out in an MBraun glovebox under a nitrogen atmosphere or using standard Schlenk techniques. Ethereal solvents, pentane, and toluene were purchased from Aldrich Chemical Co. and purified by passing through alumina columns to remove water after sparging with dinitrogen to remove oxygen. Benzene and chloroform was purchased from Aldrich Chemical Co. and sparged with dry dinitrogen and distilled from CaH_2 before use. Ammonium metavanadate, $TiCl_4$, and PMe_3 were purchased from Aldrich Chemical Co. and used as received. Hexamethyldisilazane was purchased from Oakwood Chemical and distilled under dry nitrogen before use. Pyridine, 4-methylpyridine and 4-*tert*-butylpyridine were purchased from Aldrich Chemical Co., sparged with dry dinitrogen and distilled from CaH_2 before use. 4-Dimethylaminopyridine was purchased from Aldrich Chemical Co. and pumped off in a glovebox overnight before using. Diisopropylamine was purchased from Aldrich Chemical Co. and purified by passing it over a neutral alumina column under N_2 and stored over 3 Å molecular sieves. $KOSiPh_3$ was prepared according to literature procedures.[17] Potassium pyridine-2-carboxylate was synthesized by addition of 1 equivalent of potassium hydride to 2-picolinic acid in THF. The solution was stirred under room temperature for 2 days and the solvent removed under vacuum to yield potassium pyridine-2-carboxylate as a colorless solid.

All NMR solvents were purchased from Cambridge Isotopes Laboratories, Inc. Deuterated chloroform and benzene were distilled from CaH_2 and stored over 3 Å molecular sieves in the glove box. Spectra were taken on Varian instruments located in the Max T. Rogers Instrumentation Facility at Michigan State University. These include a UNITYplus 500 spectrometer equipped with a 5 mm pulsed-field-gradient (PFG) switchable broadband probe and

operating at 499.955 MHz (^{1}H) and 125.77 MHz (^{13}C). Chemical shifts of ^{51}V NMR are reported in ppm relative to neat V(O)Cl_3 (131.6 mhZ, ^{51}V NMR). Single crystal X-ray diffraction data was collected in the Center for Crystallographic Research at MSU.

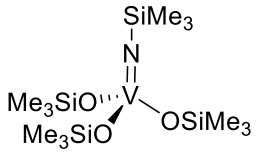

1

Synthesis of $Me_3SiN{=}V(OSiMe_3)_3$ (**1**):[13] Under N_2, a 100 mL Schlenk flask equipped with a Teflon-coated stir bar was loaded with ammonium metavanadate (4 g, 34.188 mmol) and hexamethyldisilazane (40 mL). The mixture was heated at 130 °C for 12 h. After 12 h, the black solution was cooled to room temperature, and the extra hexamethyldisilazane was removed in vacuo. The residue black oil was distilled under vacuum (137 °C). A light-yellow solid was obtained. (10.2 g, 25.185 mmol, 74%). ^{1}H NMR (C_6D_6, 500 MHz, 25 °C): 0.30 (s, 27H), 0.18 (s, 9H). ^{13}C{^{1}H} NMR (C_6D_6, 125 MHz, 25 °C): 2.1, 1.2.

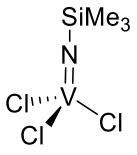

2

Synthesis of $Me_3SiN{\equiv}VCl_3$ (**2**): In a glovebox, a 20 mL scintillation vial equipped with a Teflon-coated stir bar was loaded with $Me_3SiN{=}V(OSiMe_3)_3$ (**1**) (1 g, 2.469 mmol) and pentane (2 mL). This solution was stirred at room temperature for 5 min to form a light-yellow solution. In a separate 20 mL scintillation vial, $TiCl_4$ (0.7 g, 3.690 mmol) was mixed with pentane (2 mL). The $TiCl_4$ solution was then added dropwise to the stirred solution of $Me_3SiN{=}V(OSiMe_3)_3$. During addition, the solution turned orange. Upon complete addition, the solution was stirred for 2 h at room temperature. After 2 h, the dark orange solution was reduced to 2 mL in vacuo and

stored at -35 °C for 6 h to give orange crystals of product. Further purification was achieved by one or two additional recrystallizations from pentane if necessary. (314 mg, 1.284 mmol, 52%). ^{1}H NMR (C_6D_6, 500 MHz, 25 °C): -0.09 (s, 9H). ^{13}C{^{1}H} NMR (C_6D_6, 125 MHz, 25 °C): -1.5.

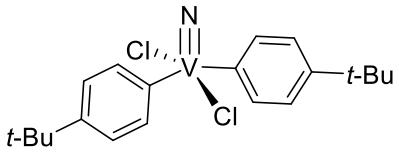

3

Synthesis of N≡VCl$_2$(4-t-bupy)$_2$ (**3**): In a glovebox, a 20 mL scintillation vial equipped with a Teflon-coated stir bar was loaded with $Me_3SiN{=}VCl_3$ (**2**) (245 mg, 1.0 mmol) and benzene (10 mL). This solution was stirred at room temperature for 5 min to form an orange solution. A solution of 4-*tert*-butylpyridine (270 mg, 2.0 mmol) in benzene (15 mL) was added dropwise. During addition, the solution turned red. Upon complete addition, the solution was stirred for 30 min at room temperature producing a deep red solution. After 30 min, solvents were removed in vacuo. The dark red powder was recrystallized in toluene/pentane. Red crystals of **3** were collected and dried under vacuum. (280 mg, 0.69 mmol, 69%). ^{1}H NMR (C_6D_6, 500 MHz, 25 °C): 9.19 (d, J=6.1Hz, 2H), 6.66 (d, J=6.1Hz, 2H), 0.79(s, 9H). ^{13}C{^{1}H} NMR (C_6D_6, 125 MHz, 25 °C): 163.6, 152.0, 121.7, 34.8, 29.8.

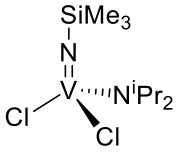

4

Synthesis of Me$_3$SiN=VCl$_2$(NiPr$_2$) (**4**): In a glovebox, a 20 mL scintillation vial equipped with a Teflon-coated stir bar was loaded with $Me_3SiN{=}VCl_3$ (**2**) (245 mg, 1.0 mmol) and toluene (5 mL). This solution was stirred at room temperature for 5 min to form an orange solution. The

solution was stirred vigorously, and HN^iPr_2 (3 mL, 21.4 mmol) was added dropwise over 5 min. During addition, the solution turned dark red. Upon complete addition, the solution was stirred for 2 h at room temperature. The volatiles were removed in vacuo. The dark red solid was extracted with pentane and filtered through Celite. The resulting filtrate was condensed to 3 mL and stored at -30 °C for 12 h. Diffraction quality dark red crystals of **4** were obtained. (219 mg, 0.71 mmol, 71%). ^{1}H NMR ($CDCl_3$, 500 MHz, 25 °C): 5.80 (hept, J = 6.3 Hz, 1H), 3.64 (s, br, 1H), 1.68 (d, J = 6.4 Hz, 6H), 1.24 (d, J = 6.3 Hz, 6H), 0.39(s, 9H). $^{13}C\{^1H\}$ NMR ($CDCl_3$, 125 MHz, 25 °C): 59.2, 57.0, 28.8, 19.2, 0.6. ^{51}V NMR (131.6 MHz, C_6D_6): -88.4. Anal. Calcd for $C_9H_{23}Cl_2N_2SiV$: C, 34.96; H, 7.50; N, 9.06. Found: C, 34.95; H, 7.64; N, 9.00. M.p.: 70.0-70.8 °C.

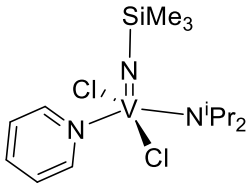

4-Py

Synthesis of $Me_3SiN{=}VCl_2(NiPr_2)(Pyridine)$ (**4-Py**): In a glovebox, a 20 mL scintillation vial equipped with a Teflon-coated stir bar was loaded with $Me_3SiN{=}VCl_2(NiPr_2)$ (**4**) (200 mg, 0.649 mmol) and pentane (5 mL). This solution was stirred at room temperature for 5 min to form a dark red solution. In another 20 mL scintillation vial, pyridine (56 mg, 0.714 mmol, 1.1 equiv.) was dissolved in pentane (5 mL). The resulting solution was added dropwise to the solution of **4** over 5 min. Upon complete addition, the solution was stirred for 2 h at room temperature, forming a red solution. The resulting red solution was then concentrated to 3 mL and stored at -30 °C for 12 h. Diffraction quality dark red crystals of **4-Py** were obtained. (229 mg, 0.591 mmol, 91%). ^{1}H NMR ($CDCl_3$, 500 MHz, 25 °C): 8.67 (s, br, 3H), 7.65 (s, br, 2H), 5.31 (hept, J = 6.2 Hz, 1H), 3.72 (hept, J = 6.2 Hz, 1H), 1.71 (d, J = 6.4 Hz, 6H), 1.23 (d, J = 6.3

Hz, 6H), 0.29 (s, 9H). $^{13}C\{^{1}H\}$ NMR ($CDCl_3$, 125 MHz, 25 °C): 150.1, 136.3, 123.8, 59.4, 56.6, 28.5, 22.4, 17.8, 14.1, 0.6. ^{51}V NMR (131.6 MHz, C_6D_6): -93.1. M.p.: 58.2-59.5 °C.

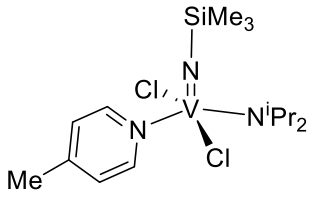

4-Mepy

Synthesis of $Me_3SiN{=}VCl_2(NiPr_2)$(4-methylpyridine) (**4-Mepy**): This material was synthesized in a manner similar to that used to prepare **4-Py** starting from $Me_3SiN{=}VCl_2(NiPr_2)$ (**4**) (100 mg, 0.324 mmol) and 4-methylpyridine (33 mg, 0.356 mmol, 1.1 equiv.); this yielded light yellow crystals of **4-Mepy** 121 mg (0.301 mmol, 93%). ^{1}H NMR (C_6D_6, 500 MHz, 25 °C): 8.82 (s, br, 2H), 6.54 (s, br, 2H), 5.51 (hept, J = 6.2 Hz, 1H), 3.25 (s, br, 1H), 1.72 (s, br, 3H), 1.59 (d, J = 6.2 Hz, 6H), 1.01 (d, J = 6.3 Hz, 6H), 0.21 (s, 9H). $^{13}C\{^{1}H\}$ NMR (C_6D_6, 125 MHz, 25 °C): 150.8, 147.8, 124.5, 59.0, 57.2, 28.6, 20.5, 17.9, 0.5. ^{51}V NMR (131.6 MHz, C_6D_6): -133.2. M.p.: 71.0-72.0 °C.

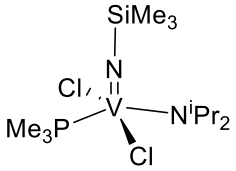

4-PMe$_3$

Synthesis of $Me_3SiN{=}VCl_2(NiPr_2)(PMe_3)$ (**4-PMe$_3$**): This material was synthesized in a manner similar to that used to prepare **4-Py** starting from $Me_3SiN{=}VCl_2(NiPr_2)$ (**4**) (100 mg, 0.324 mmol) and PMe_3 (27 mg, 0.356 mmol, 1.1 equiv.); this yielded pink crystals of **4-PMe$_3$** 103 mg (0.268 mmol, 83%). ^{1}H NMR (C_6D_6, 500 MHz, 25° C): 5.37 (hept, J = 6.3 Hz, 1H), 3.21 (hept, J = 6.3 Hz, 1H), 1.54 (d, J = 6.4 Hz, 6H), 1.28 (s, br, 3H), 0.98 (d, J = 6.3 Hz, 6H), 0.20(s,

9H). $^{13}C\{^{1}H\}$ NMR (C_6D_6, 125 MHz, 25 °C): 58.4, 56.4, 28.6, 17.9, 0.8. ^{51}V NMR (131.6 MHz, C_6D_6): -115.5. M.p.: 74.3-76.0 °C.

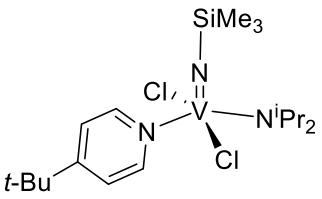

4-^{t}bupy

Synthesis of $Me_3SiN{=}VCl_2(NiPr_2)$(4-t-butylpyridine) (**4-^{t}bupy**): This material was synthesized in a manner similar to that used to prepare **4-Py** starting from $Me_3SiN{=}VCl_2(NiPr_2)$ (**4**) (200 mg, 0.649 mmol) and 4-*tert*-butylpyridine (96 mg, 0.714 mmol, 1.1 equiv.); this yielded red solid of **4-^{t}bupy** 264.2 mg (0.595 mmol, 92%). ^{1}H NMR (C_6D_6, 500 MHz, 25 °C): 8.85(s, br, 2H), 6.85(s, br, 2H), 5.55 (hept, J = 6.3 Hz, 1H), 3.26 (s, br, 1H), 1.58 (d, J = 6.2 Hz, 6H), 1.00 (d, J = 6.2 Hz, 6H), 0.97(s, 9H), 0.21(s, 9H). $^{13}C\{^{1}H\}$ NMR (C_6D_6, 125 MHz, 25 °C): 159.8, 150.7, 120.6, 59.0, 57.2, 34.4, 30.3, 28.6, 17.8, 0.6. ^{51}V NMR (131.6 MHz, C_6D_6): -112.3.

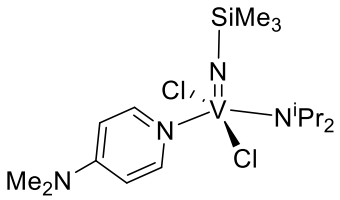

4-DMAP

Synthesis of $Me_3SiN{=}VCl_2(NiPr_2)$(4-dimethylaminopyridine) (**4-DMAP**): In a glovebox, a 20 mL scintillation vial equipped with a Teflon-coated stir bar was loaded with $Me_3SiN{=}VCl_2(NiPr_2)$ (**4**) (200 mg, 0.649 mmol) and chloroform (2 mL). This solution was stirred at room temperature for 5 min to form a dark red solution. In another 20 mL scintillation vial, 4-dimethylaminopyridine (79 mg, 0.649 mmol, 1.0 equiv.) was dissolved in chloroform (2 mL). The resulting solution was added dropwise to the solution of **4** over 5 min. Upon complete

addition, the solution was stirred for 2 h at room temperature, forming a light orange solution. The resulting light orange solution was then concentrated to 1 mL, layered with 2 mL pentane, and stored at -30 °C for 12 h. Diffraction quality yellow crystals of **4- DMAP** were obtained. (129 mg, 0.299 mmol, 46%). ^{1}H NMR (C_6D_6, 500 MHz, 25 °C): 9.03 (s, br, 2H), 5.95 (s, br, 2H), 5.29 (hept, J = 5.9 Hz, 1H), 3.46 (hept, J = 6.1 Hz, 1H), 2.10 (s, 3H), 1.79 (d, J = 6.4 Hz, 6H), 1.18 (d, J = 6.2 Hz, 6H), 0.28 (s, 9H). ^{13}C{^{1}H} NMR (C_6D_6, 125 MHz, 25 °C): 154.4, 151.4, 105.8, 59.0, 57.0, 38.2, 28.8, 23.8, 17.3, 0.7. ^{51}V NMR (131.6 MHz, C_6D_6): -144.5.

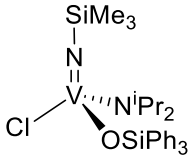

5

Synthesis of $Me_3SiN{=}VCl(N^iPr_2)(OSiPh_3)$ (**5**): In a glovebox, a 20 mL scintillation vial equipped with a Teflon-coated stir bar was loaded with $Me_3SiN{=}VCl_2(NiPr_2)$(pyridine) (**4-Py**) (100.0 mg, 0.258 mmol) and THF (5 mL). The resulting red solution was cooled to nearly frozen. $KOSiPh_3$ (81 mg, 0.258 mmol, 1.0 equiv.) was slowly added to the resulting solution. The solution turned a pink color upon completion of the addition. After stirring at room temperature for 12 h, the volatiles were removed in vacuo. The residue red solid was extracted with pentane and filtered through Celite. The resulting filtrate was condensed to 3 mL and stored at -30 °C for 12 h. Diffraction quality pink crystals of **5** were obtained. (79 mg, 0.144 mmol, 56%). ^{1}H NMR (C_6D_6, 500 MHz, 25 °C): 7.54-7.49 (m, 6H), 7.32-7.22 (m, 9H), 5.15 (hept, J = 6.3 Hz, 1H), 3.39 (s, br, 1H), 1.57 (d, J = 6.2 Hz, 3H), 1.45 (d, J = 6.2 Hz, 3H), 1.06 (d, J = 6.1 Hz, 3H), 0.77 (d, J = 6.1 Hz, 3H), -0.09 (s, 9H).

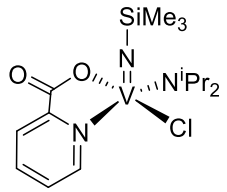

6

Synthesis of $Me_3SiN{=}VCl(N^iPr_2)$(pyridine-2-carboxylate) (**6**): In a glovebox, a 20 mL scintillation vial equipped with a Teflon-coated stir bar was loaded with $Me_3SiN{=}VCl_2(NiPr_2)$(pyridine) (**4-Py**) (100.0 mg, 0.258 mmol) and THF (5 mL). The resulting red solution was cooled to nearly frozen. Potassium pyridine-2-carboxylate (42 mg, 0.258 mmol, 1.0 equiv.) was slowly added to the resulting solution. After stirring at room temperature for 24 h, the resulting solution turned a brown color, and the volatiles were removed in vacuo. The residue dark brown solid was extracted with toluene and pumped off to 1 mL. This resulting toluene solution was layered with 2 mL pentane and stored at -30 °C for 12 h. Diffraction quality brown crystals of **6** were obtained. (65 mg, 0.165 mmol, 64%). ^{1}H NMR (C_6D_6, 500 MHz, 25 °C): 9.37 (s, 1H), 7.99 (d, J = 7.2 Hz, 1H), 6.97 (t, J = 6.8 Hz, 1H), 6.64 (s, 1H), 5.95 (s, br, 2H), 4.67 ((s, br, 2H), 3.42 (s, br, 2H), 1.73 (t, J = 6.3 Hz, 6H), 1.08 (dd, J = 21.1, 5.7 Hz, 6H), -0.13 (s, 9H). ^{13}C{^{1}H} NMR (C_6D_6, 125 MHz, 25 °C): 150.4, 149.4, 140.4, 126.7, 124.3, 58.4, 55.6, 28.9, 28.5, 17.3, 16.6, 0.1. ^{51}V NMR (131.6 MHz, C_6D_6): -249.9.

NMR Spectra

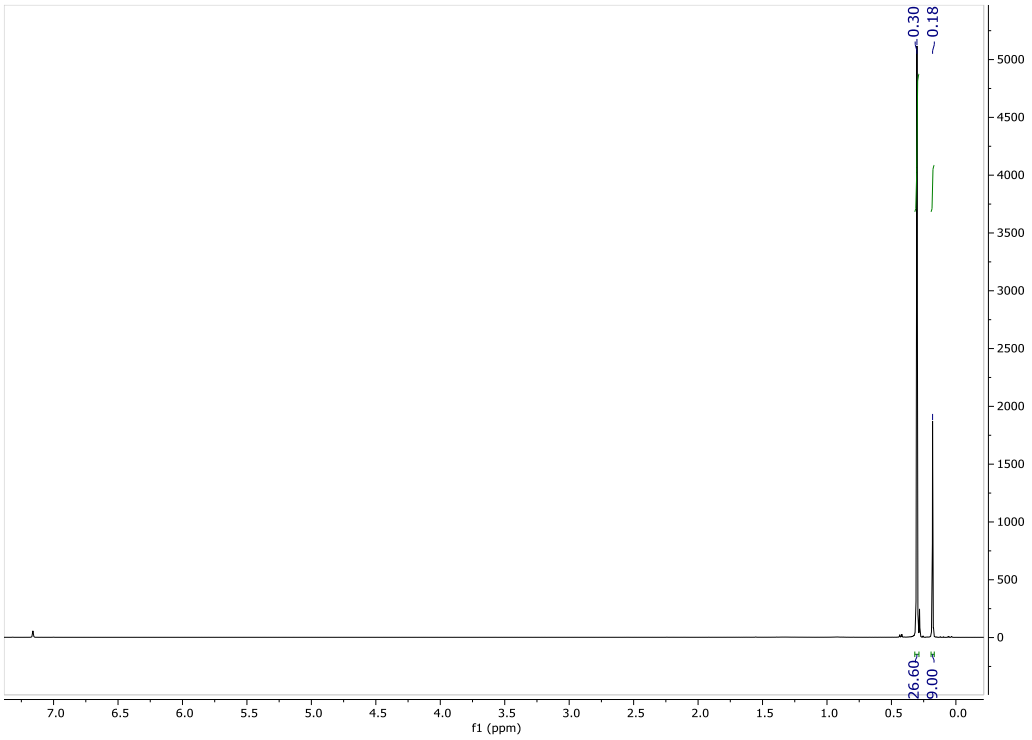

Figure 3-5. $Me_3SiN=V(OSiMe_3)_3$ (**1**) ^1H NMR C_6D_6 25 °C.

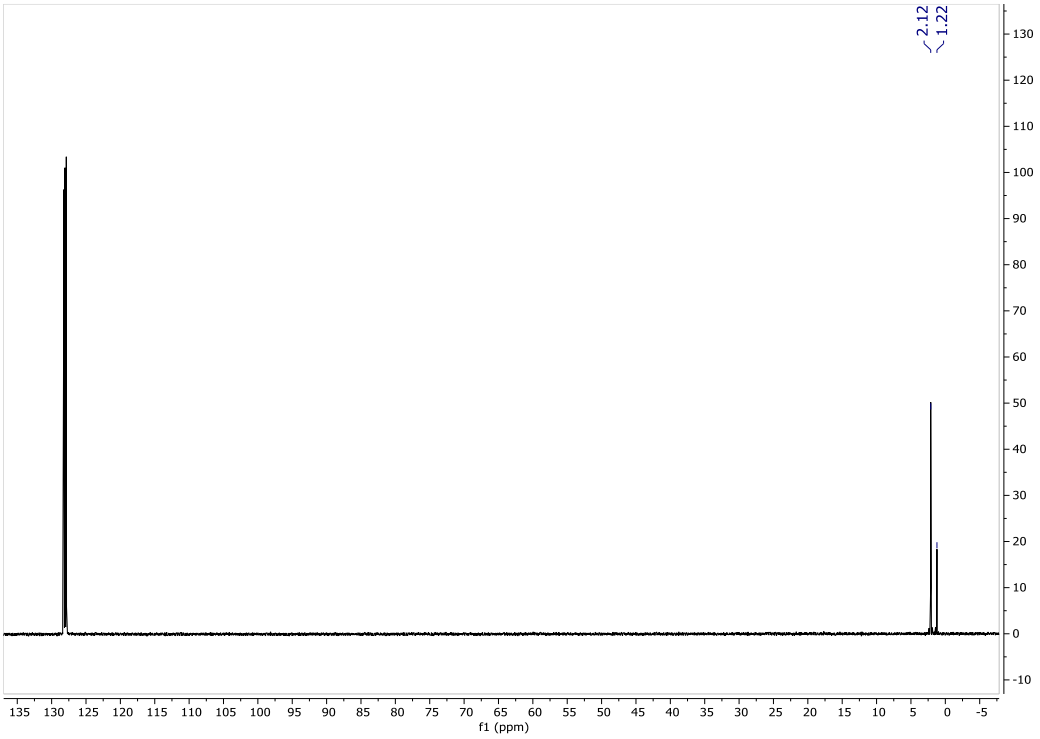

Figure 3-6. $Me_3SiN=V(OSiMe_3)_3$ (**1**) ^{13}C NMR C_6D_6 25 °C.

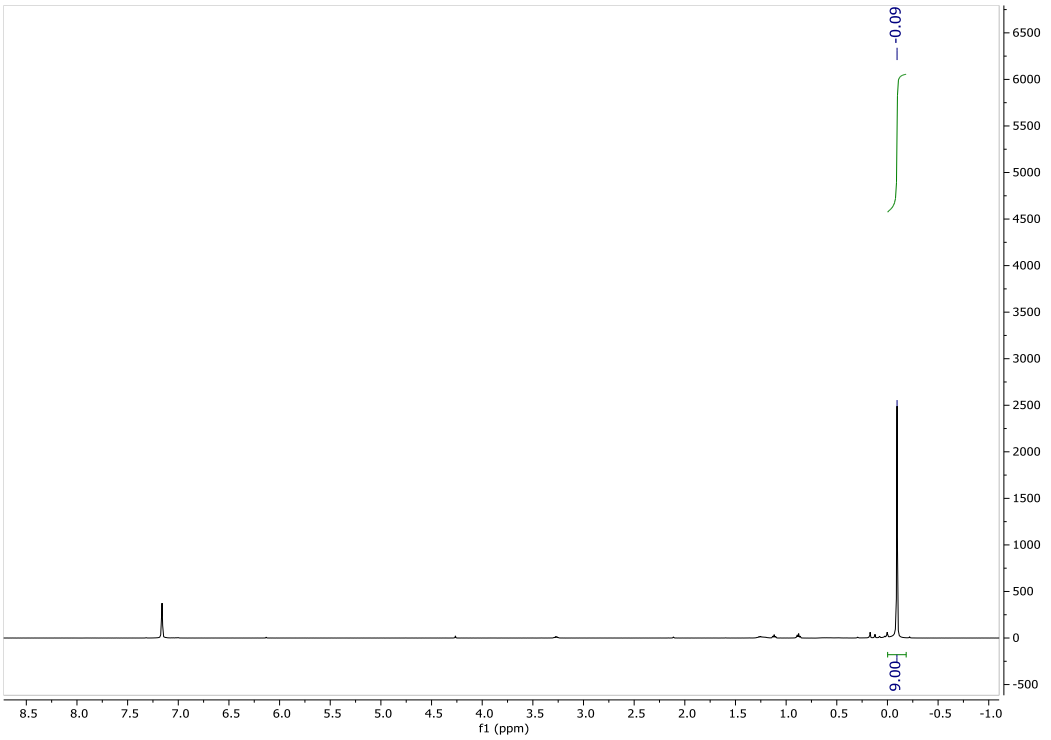

Figure 3-7. $Me_3SiN{\equiv}VCl_3$ (**2**) ^1H NMR C_6D_6 25 °C.

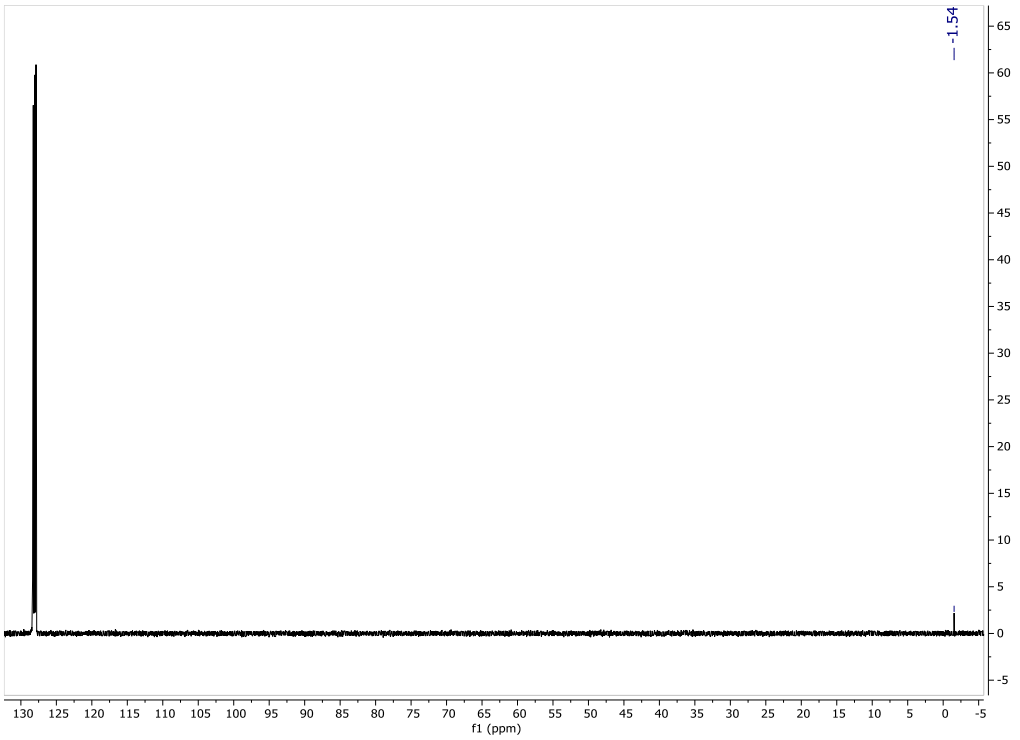

Figure 3-8. $Me_3SiN{\equiv}VCl_3$ (**2**) ^{13}C NMR C_6D_6 25 °C.

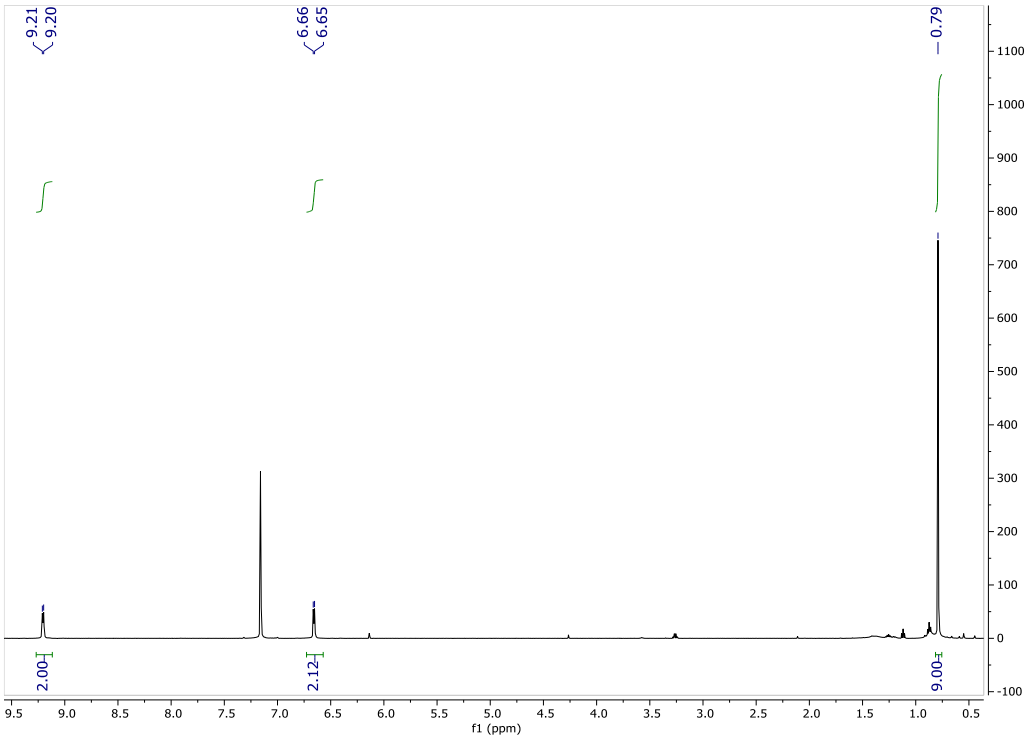

Figure 3-9. N≡VCl_2(4-*t*-bupy)$_2$ (**3**) ^{1}H NMR C_6D_6 25 °C.

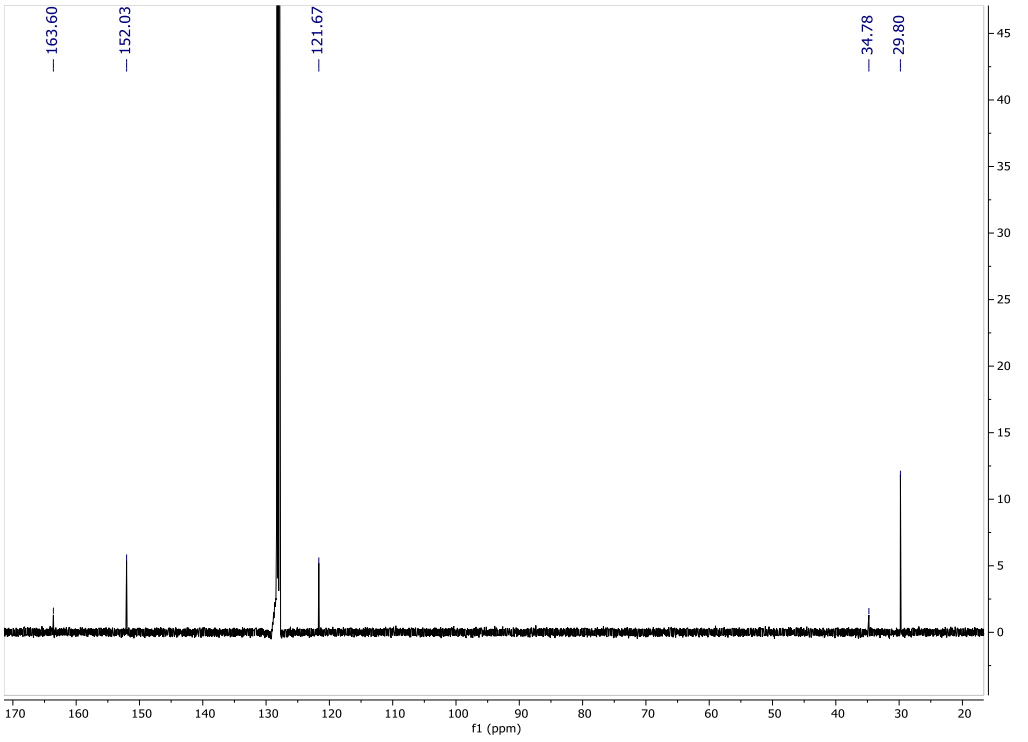

Figure 3-10. N≡VCl_2(4-*t*-bupy)$_2$ (**3**) ^{13}C NMR C_6D_6 25 °C.

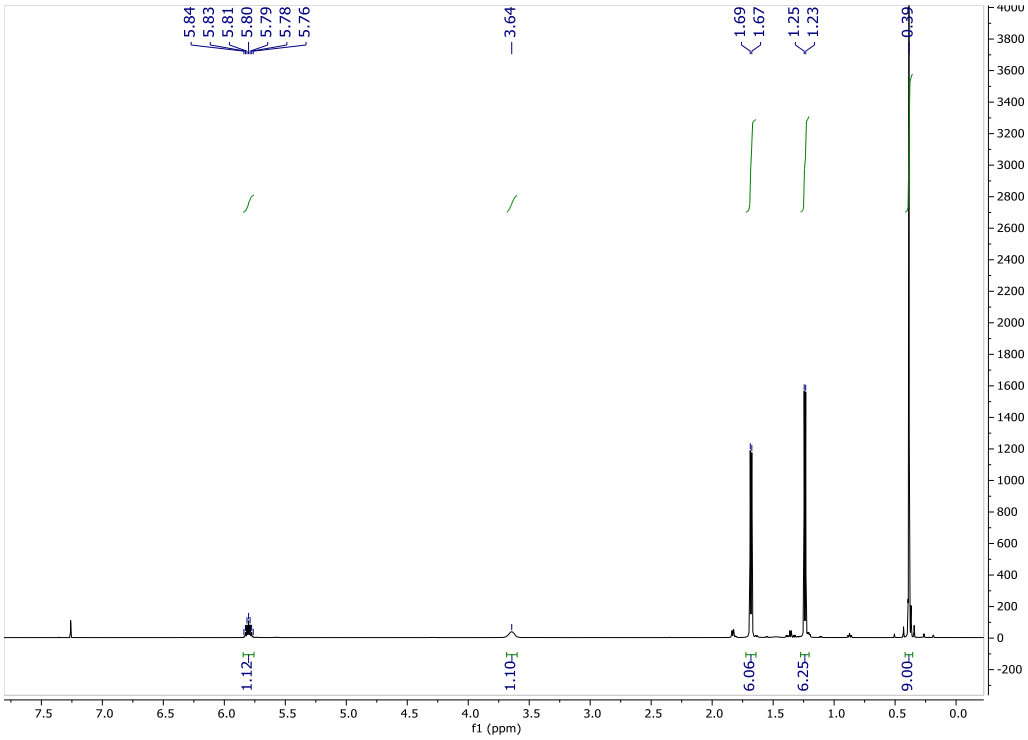

Figure 3-11. $Me_3SiN{=}VCl_2(N^iPr_2)$ (**4**) ^1H NMR $CDCl_3$ 25 °C.

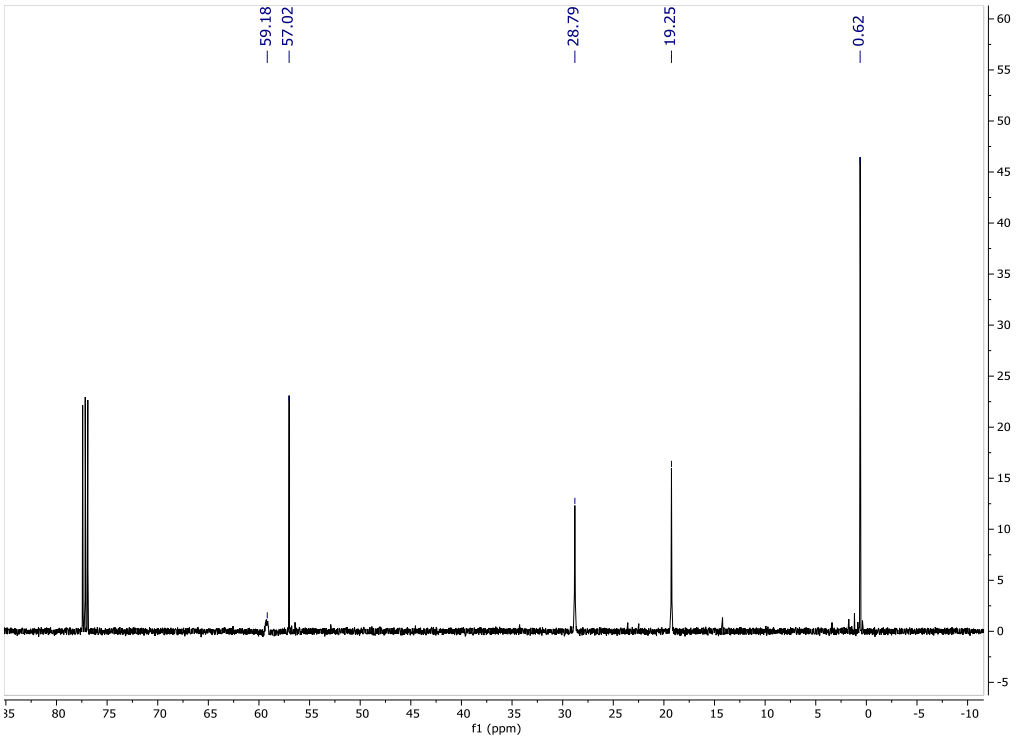

Figure 3-12. $Me_3SiN{=}VCl_2(N^iPr_2)$ (**4**) ^{13}C NMR $CDCl_3$ 25 °C.

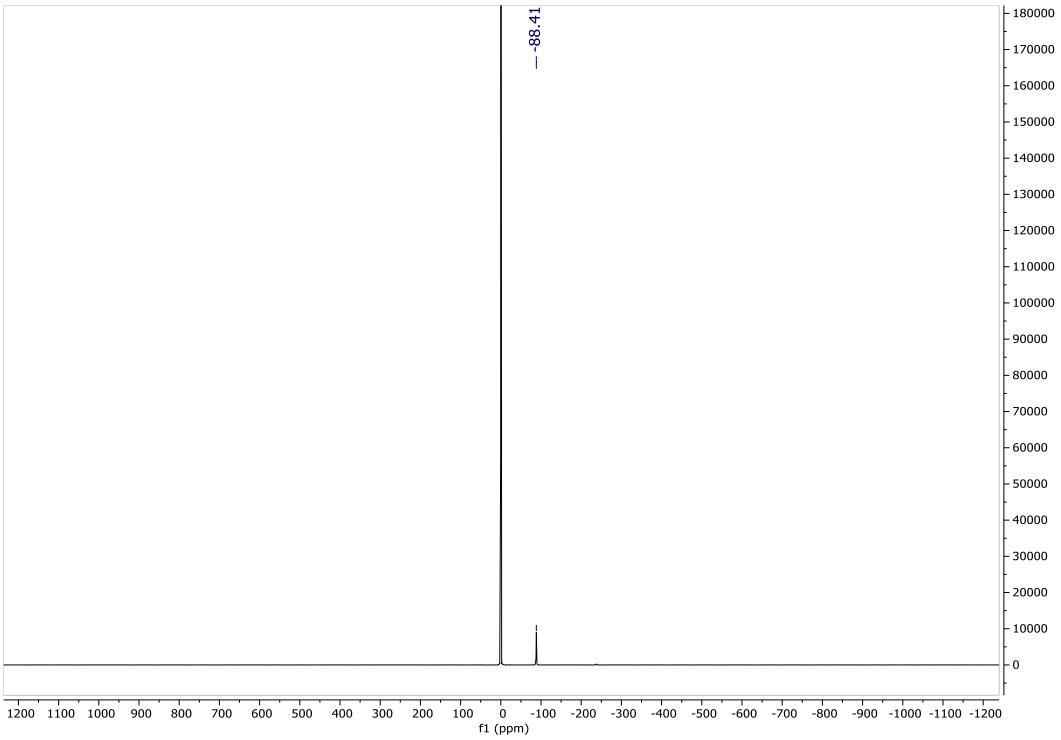

Figure 3-13. $Me_3SiN{=}VCl_2(N^iPr_2)$ (**4**) ^{51}V NMR C_6D_6 25 °C.

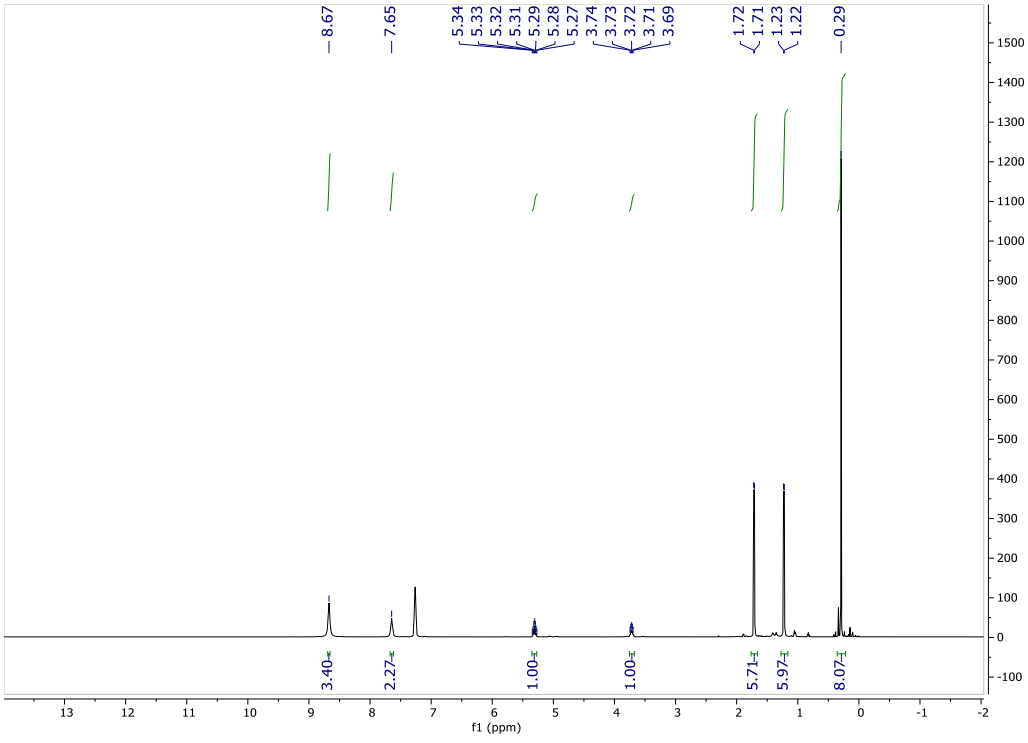

Figure 3-14. $Me_3SiN{=}VCl_2(N^iPr_2)$(pyridine) (**4-Py**) ^1H NMR $CDCl_3$ 25 °C.

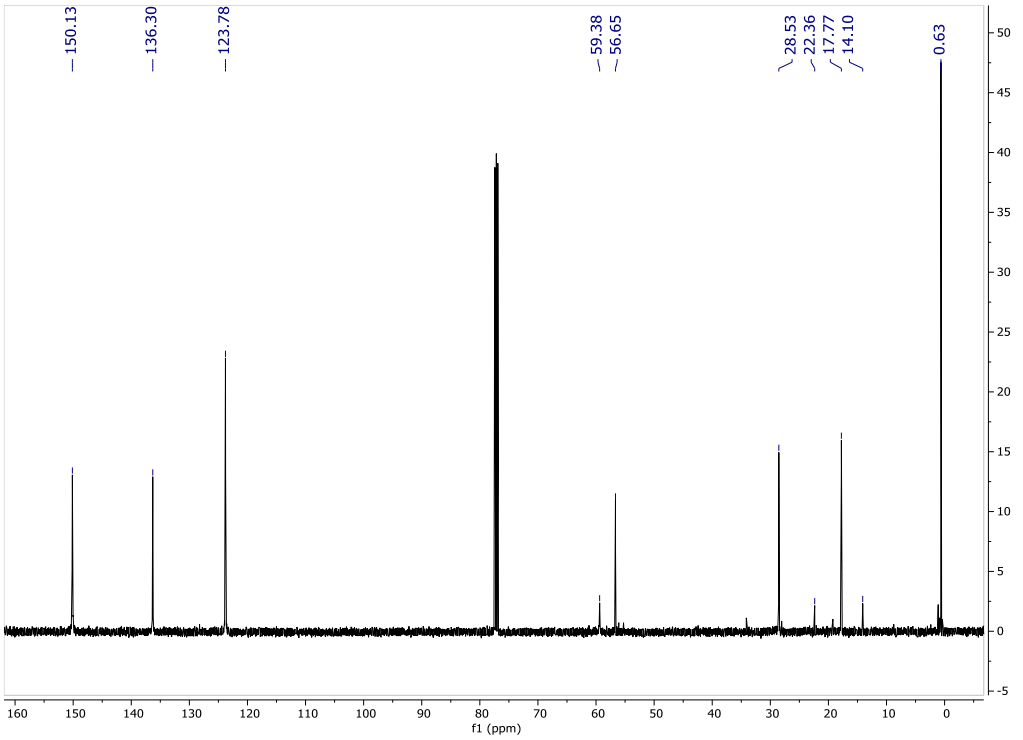

Figure 3-15. $Me_3SiN=VCl_2(N^iPr_2)$(pyridine) (**4-Py**) ^{13}C NMR $CDCl_3$ 25 °C.

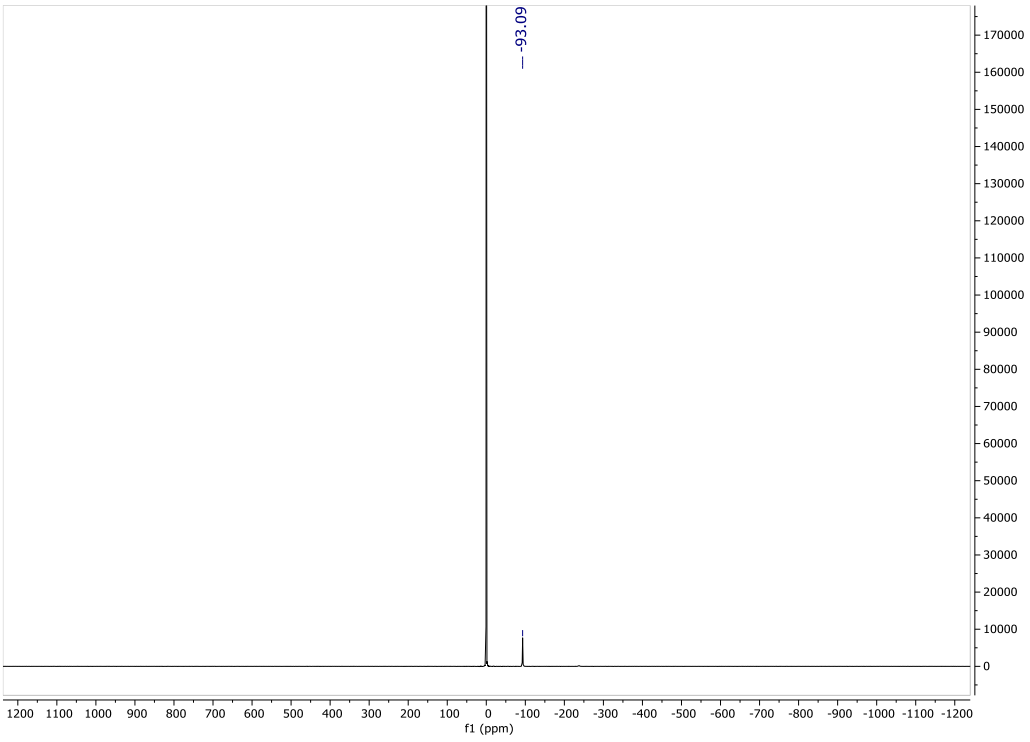

Figure 3-16. $Me_3SiN=VCl_2(N^iPr_2)$(pyridine) (**4-Py**) ^{51}V NMR C_6D_6 25 °C.

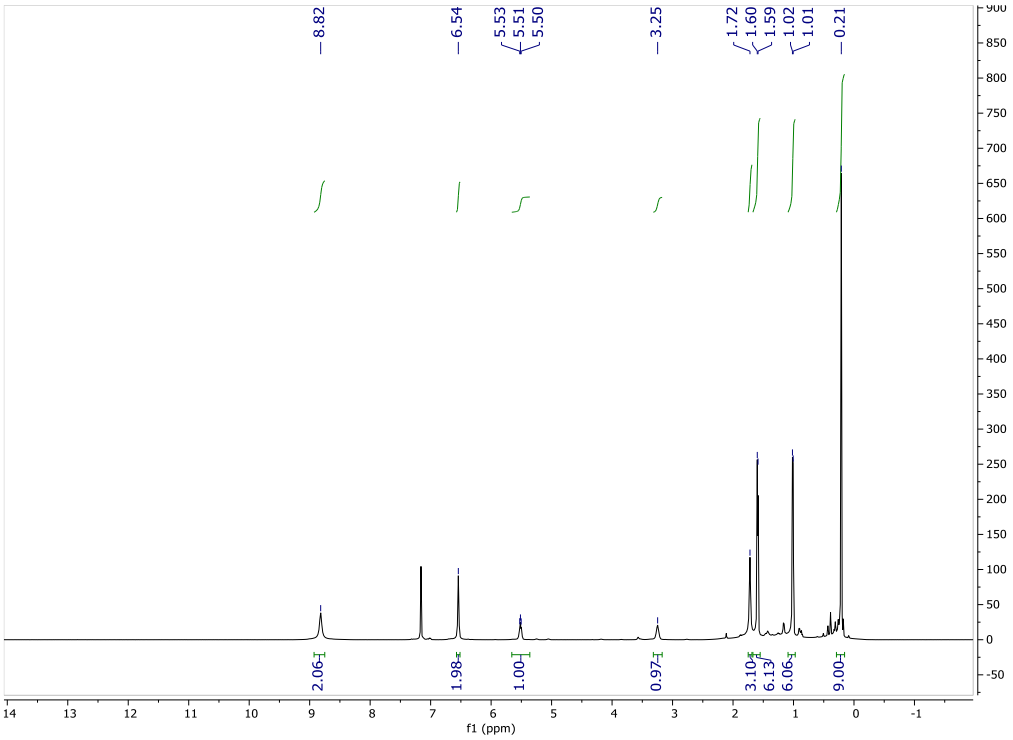

Figure 3-17. $Me_3SiN{=}VCl_2(N^iPr_2)$(4-methylpyridine) (**4-Mepy**) ^1H NMR C_6D_6 25 °C.

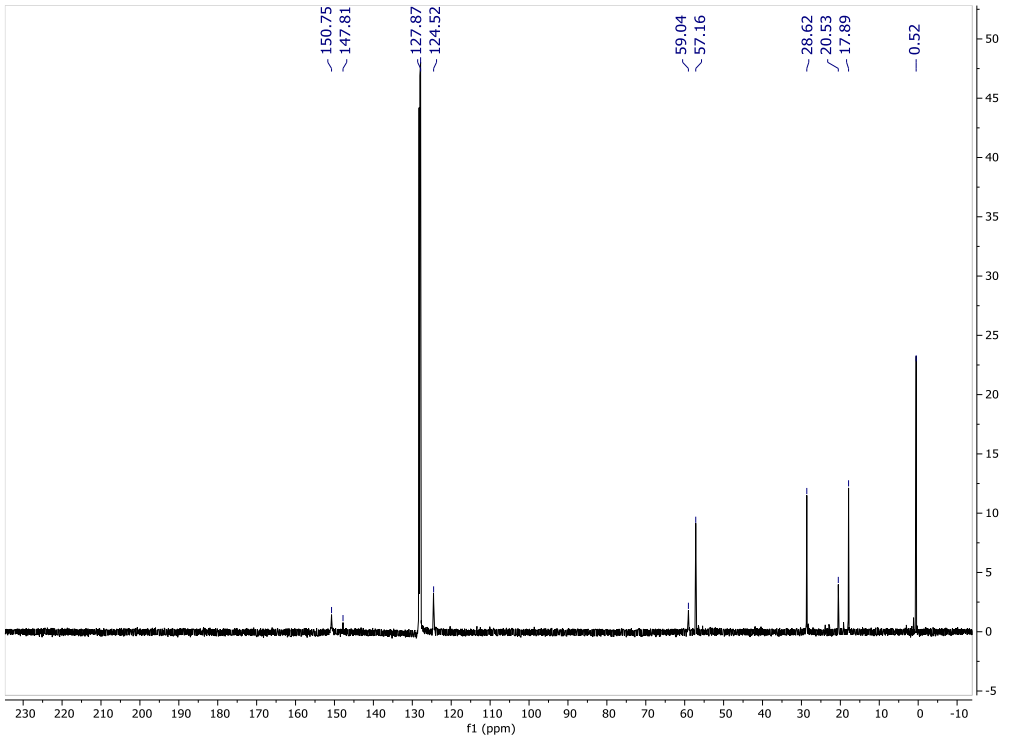

Figure 3-18. $Me_3SiN{=}VCl_2(N^iPr_2)$(4-methylpyridine) (**4-Mepy**) ^{13}C NMR C_6D_6 25 °C.

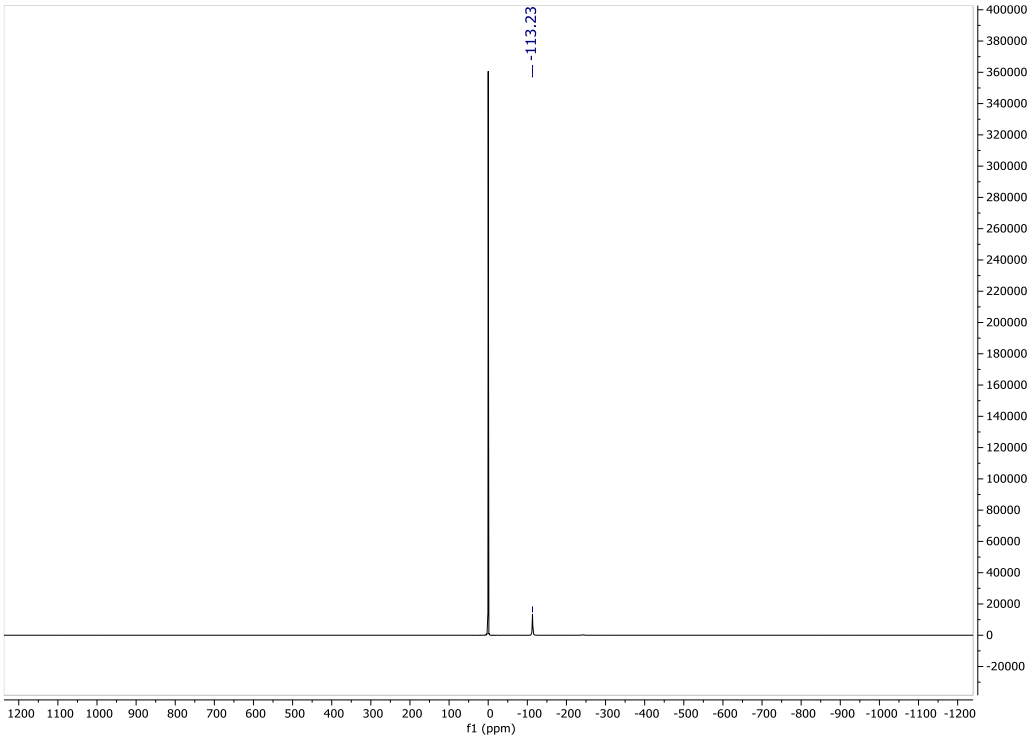

Figure 3-19. $Me_3SiN{=}VCl_2(N^iPr_2)$(4-methylpyridine) (**4-Mepy**) ^{51}V NMR C_6D_6 25 °C.

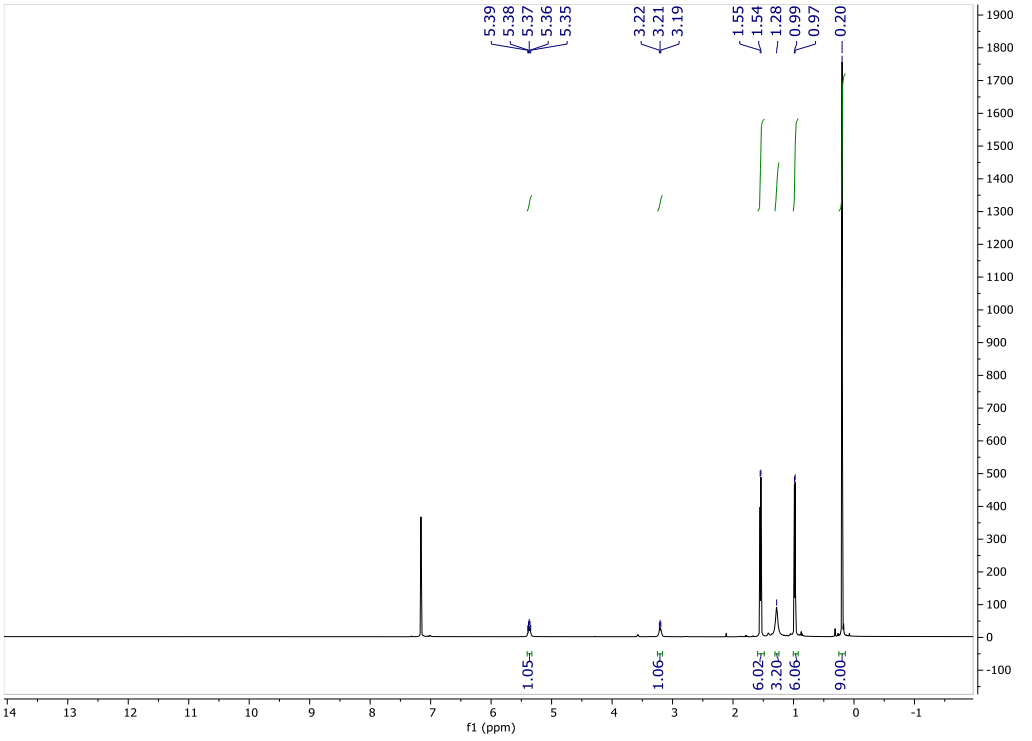

Figure 3-20. $Me_3SiN{=}VCl_2(N^iPr_2)(PMe_3)$ (**4-PMe$_3$**) ^1H NMR C_6D_6 25 °C.

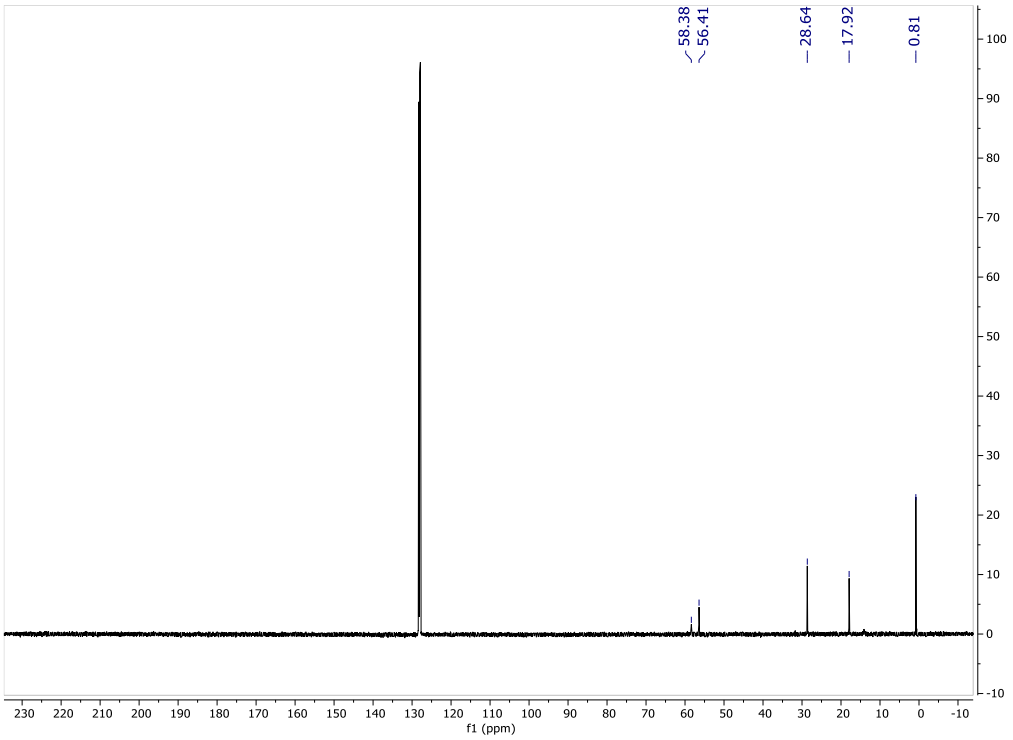

Figure 3-21. $Me_3SiN{=}VCl_2(N^iPr_2)(PMe_3)$ (**4-PMe$_3$**) ^{13}C NMR C_6D_6 25 °C.

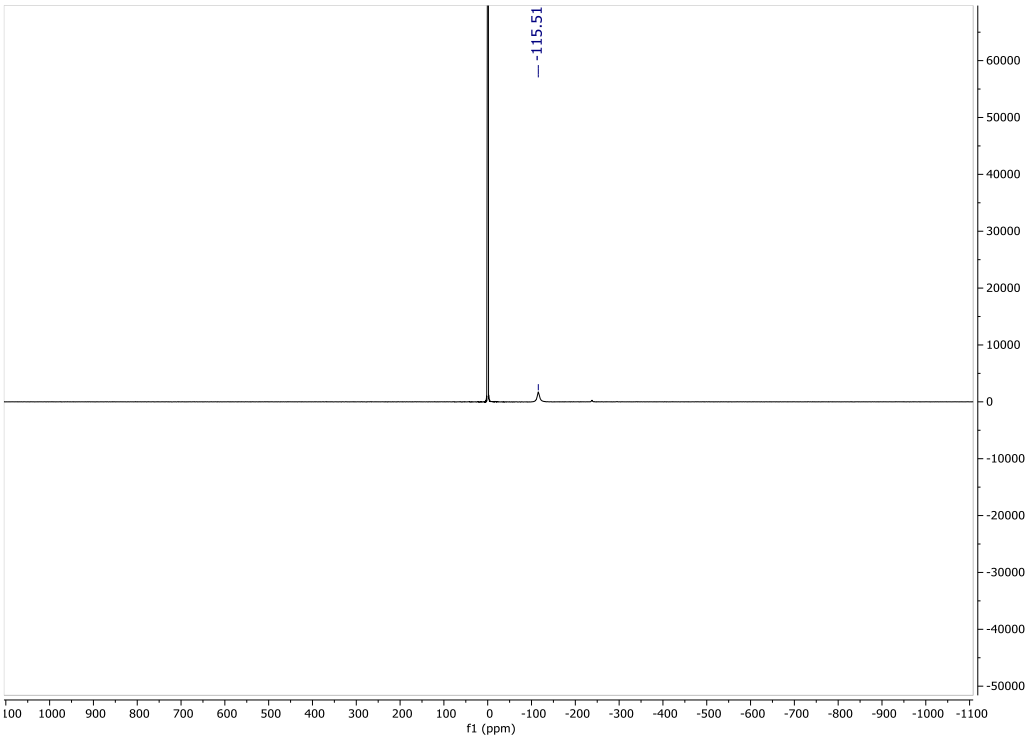

Figure 3-22. $Me_3SiN{=}VCl_2(N^iPr_2)(PMe_3)$ (**4-PMe$_3$**) ^{51}V NMR C_6D_6 25 °C.

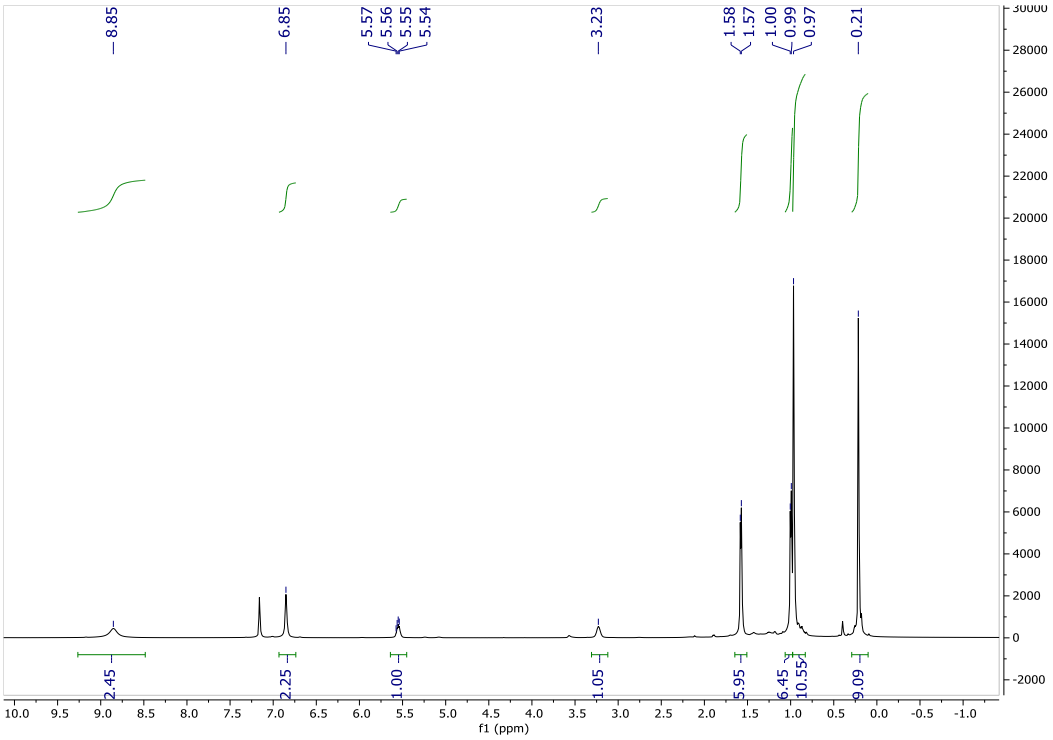

Figure 3-23. $Me_3SiN{=}VCl_2(N^iPr_2)$(4-*t*-butylpyridine) (**4-^{t}bupy**) ^{1}H NMR C_6D_6 25 °C.

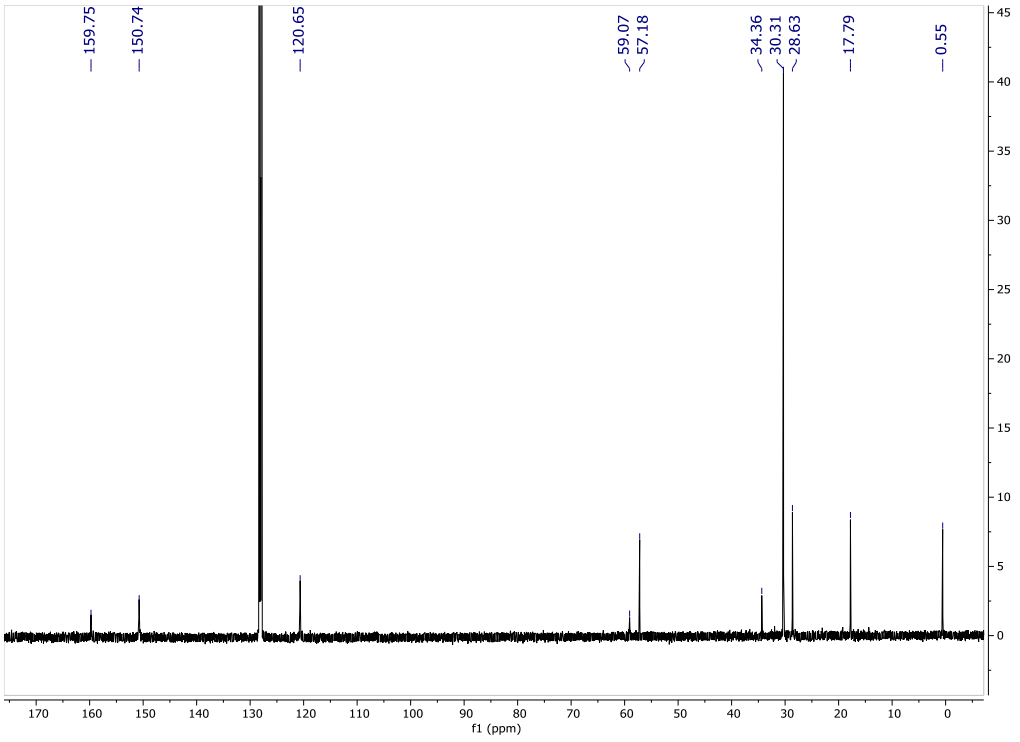

Figure 3-24. $Me_3SiN{=}VCl_2(N^iPr_2)$(4-*t*-butylpyridine) (**4-^{t}bupy**) ^{13}C NMR C_6D_6 25 °C.

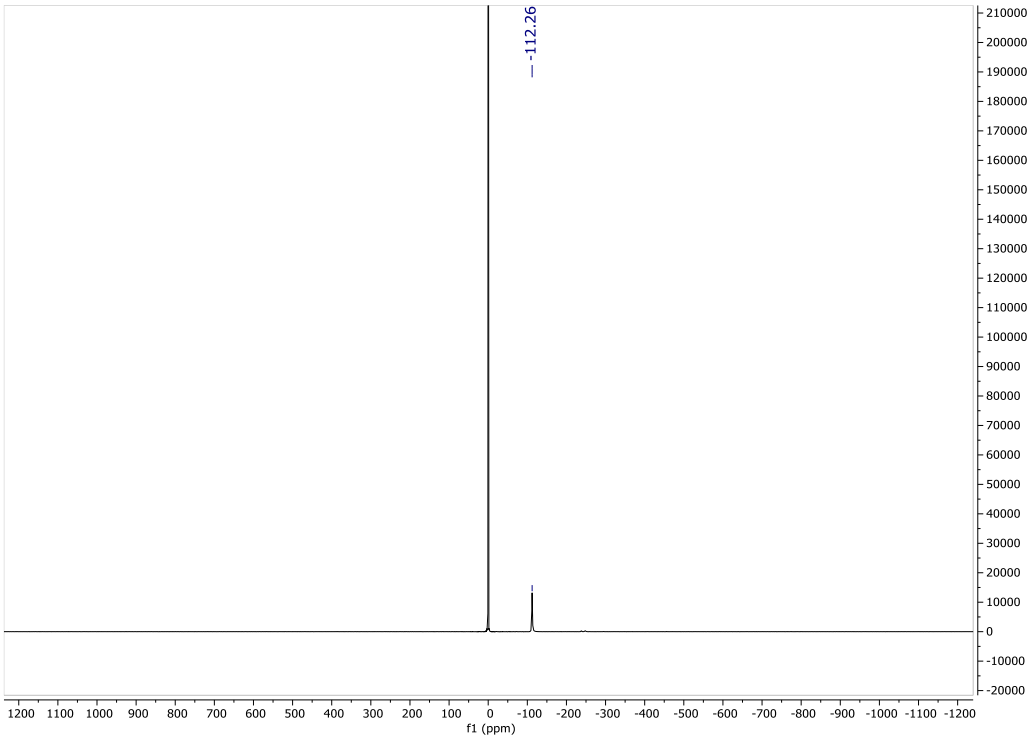

Figure 3-25. $Me_3SiN{=}VCl_2(N^iPr_2)$(4-*t*-butylpyridine) (**4-^{t}bupy**) ^{51}V NMR C_6D_6 25 °C.

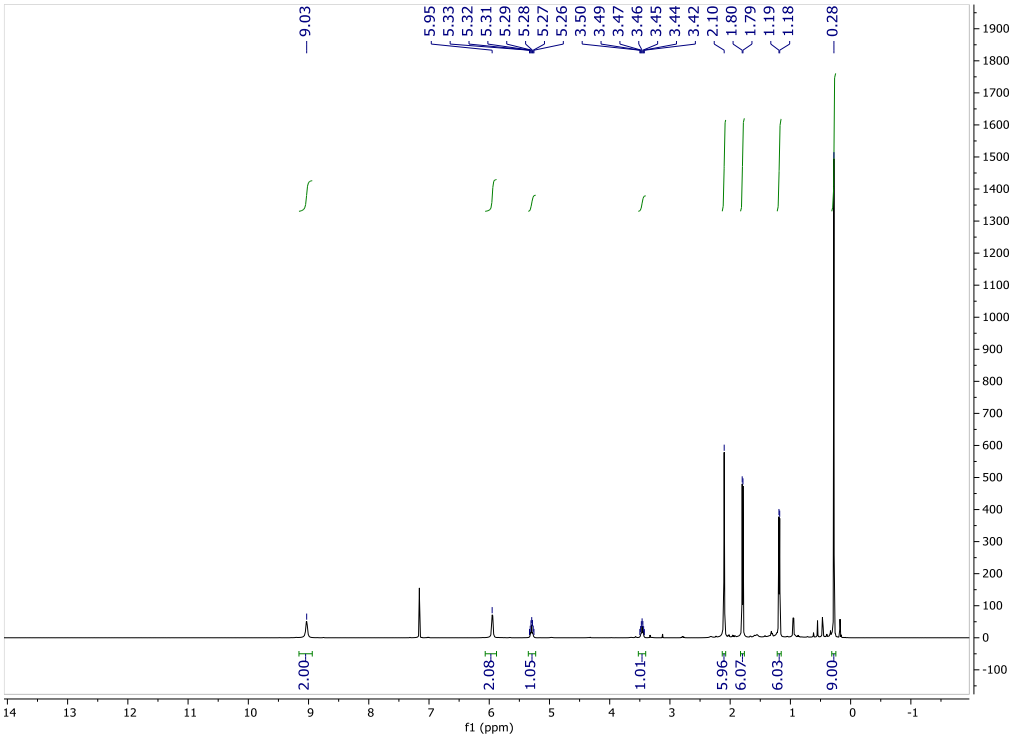

Figure 3-26. $Me_3SiN{=}VCl_2(N^iPr_2)$(4-dimethylaminopyridine) (**4-DMAP**) ^1H NMR C_6D_6 25 °C.

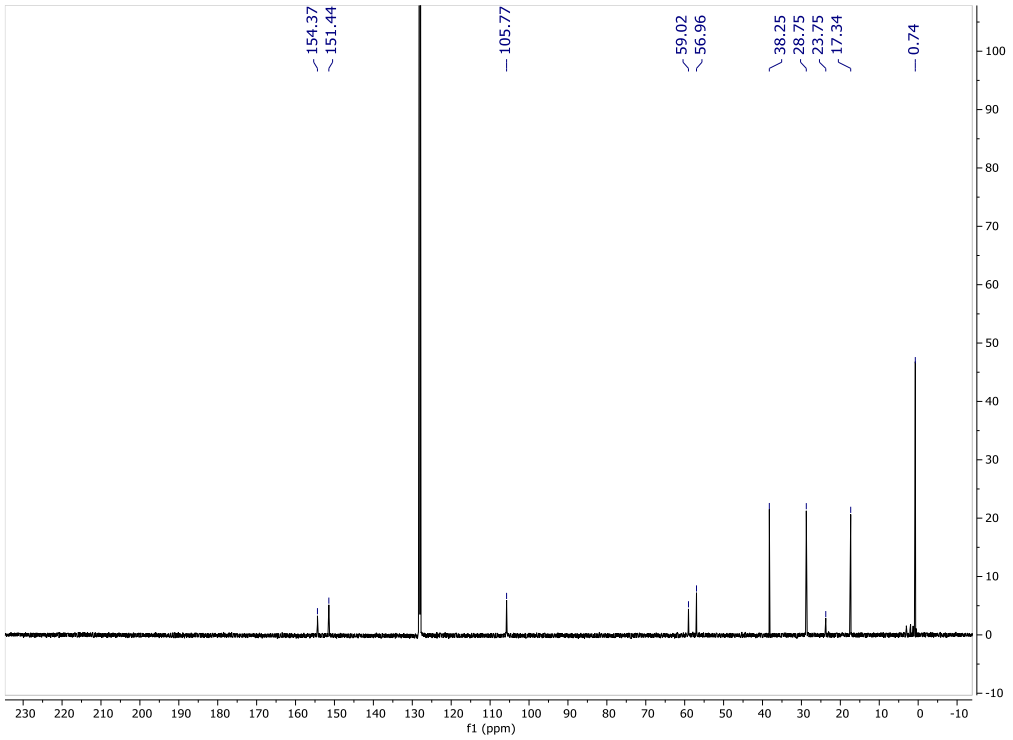

Figure 3-27. $Me_3SiN=VCl_2(N^iPr_2)$(4-dimethylaminopyridine) (**4-DMAP**) ^{13}C NMR C_6D_6 25 °C.

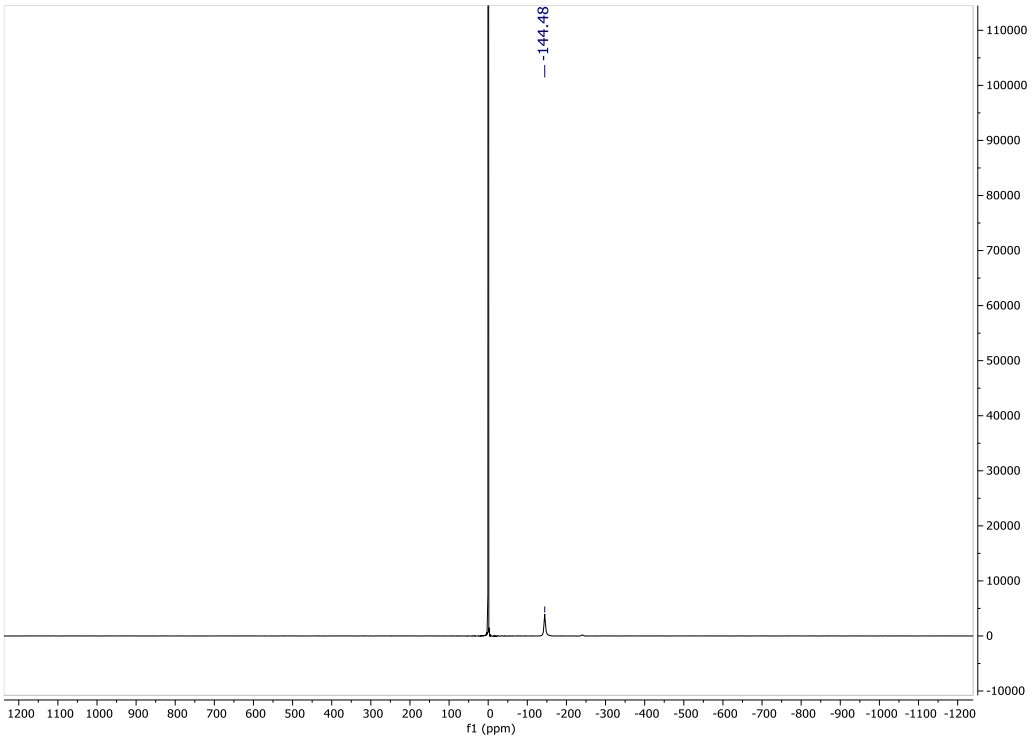

Figure 3-28. $Me_3SiN=VCl_2(N^iPr_2)$(4-dimethylaminopyridine) (**4-DMAP**) ^{51}V NMR C_6D_6 25 °C.

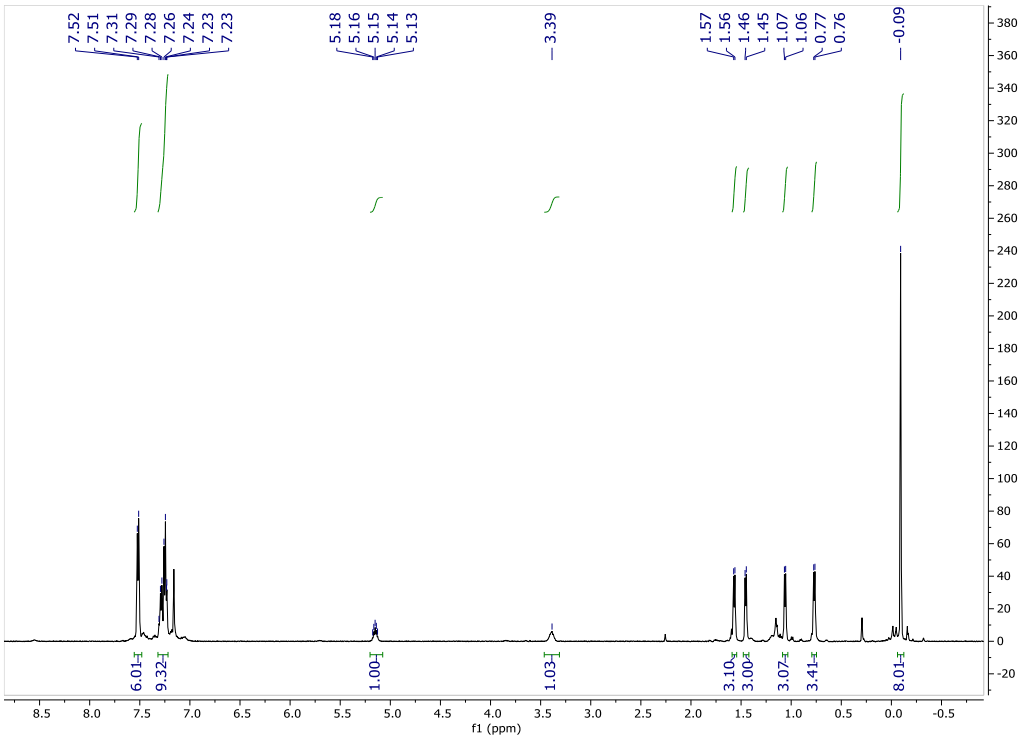

Figure 3-29. $Me_3SiN{=}VCl(N^iPr_2)(OSiPh_3)$ (**5**) ^1H NMR C_6D_6 25 °C.

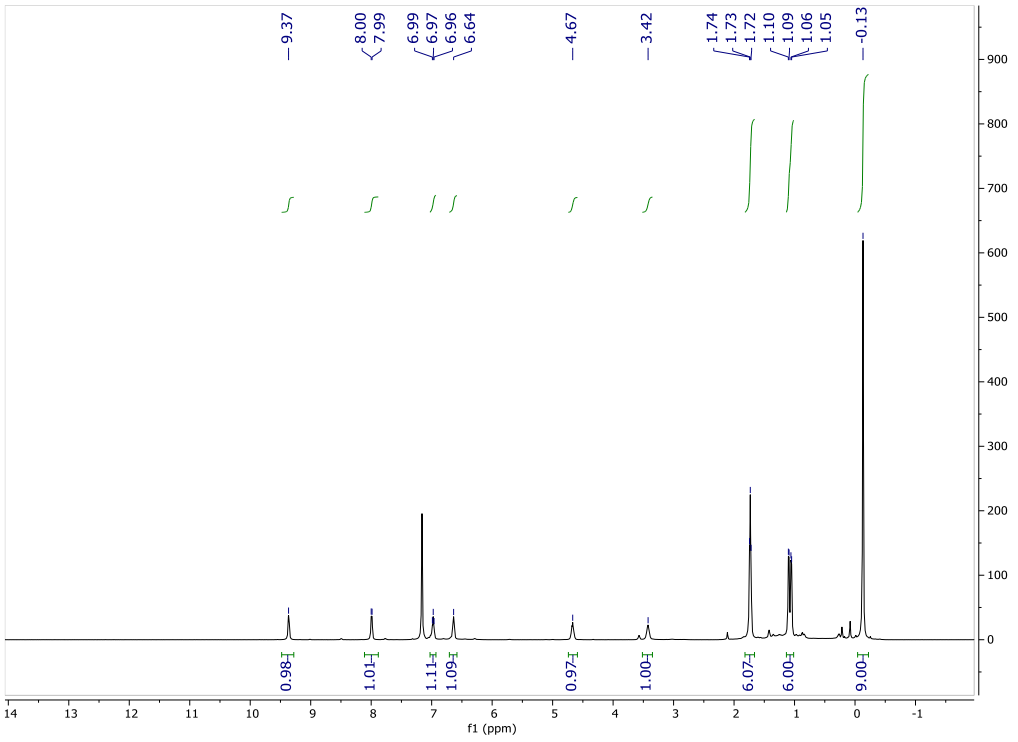

Figure 3-30. $Me_3SiN{=}VCl(N^iPr_2)$(pyridine-2-carboxylate) (**6**) ^1H NMR C_6D_6 25 °C.

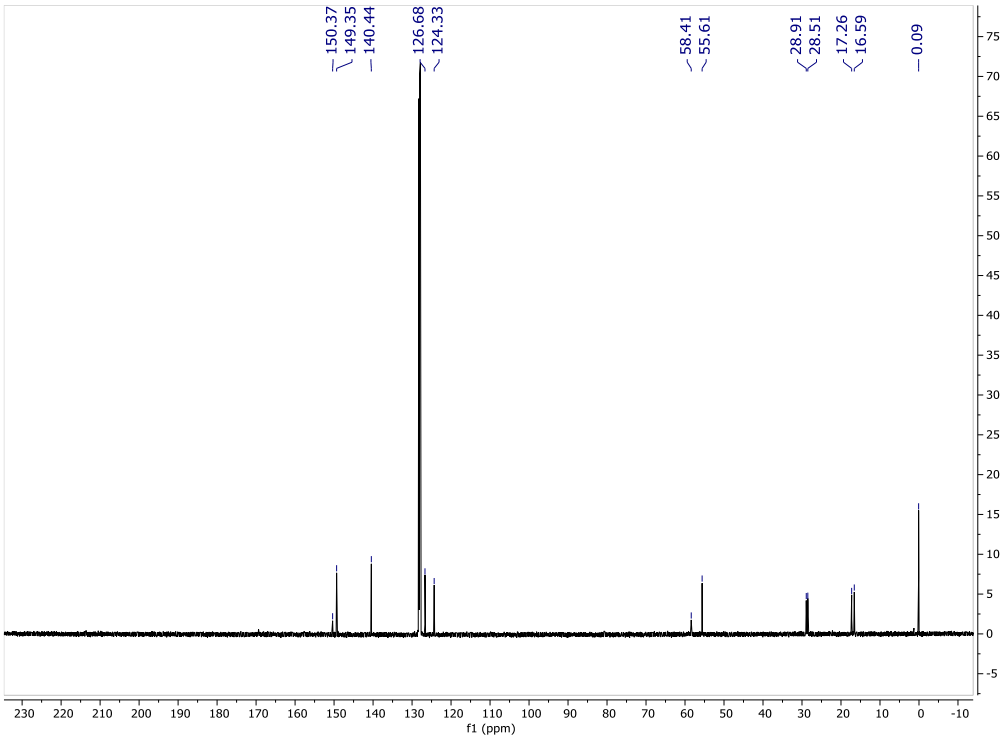

Figure 3-31. $Me_3SiN{=}VCl(N^iPr_2)$(pyridine-2-carboxylate) (**6**) ^{13}C NMR C_6D_6 25 °C.

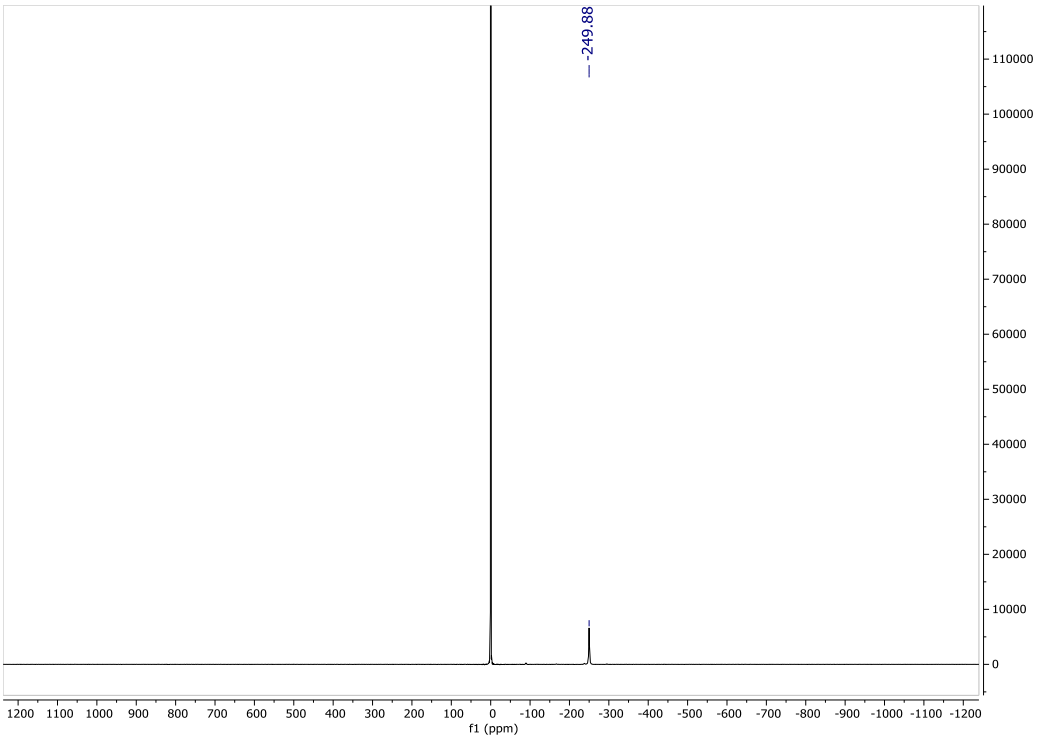

Figure 3-32. $Me_3SiN{=}VCl(N^iPr_2)$(pyridine-2-carboxylate) (**6**) ^{51}V NMR C_6D_6 25 °C.

General Considerations for LDP measurement. In this study, the rate of -N^iPr_2 rotation was determined by Spin Saturation Transfer ^1H NMR over a range of temperatures. Then Eyring equation was used to determine $\Delta S^‡$ and $\Delta H^‡$ by taking $\Delta G^‡$ as a function of temperature (K). Practically, $\ln(k_{obs}/T)$ vs. 1/T was plotted under 5 different temperatures. $\Delta H^‡$ and $\Delta S^‡$ can be derived from the slope and intercept of the Eyring plots. Standard treatment of the data was used to approximate errors in these values.

Table 3-5. Experimental Data for $\Delta H^{\ddagger}$ and $\Delta S^{\ddagger}$ measurements of **4**, **4-Py** and **4-PMe$_3$** in $CDCl_3$.

Compound No.	Temp (K)	k_{obs} (s^{-1})	$\Delta H^{\ddagger}$ (kcal/mol)	$\Delta S^{\ddagger}$ (e.u.)	$\Delta G^{\ddagger}$ (kcal/mol)
4	298.2	0.1286	19.79±0.38	3.71±1.21	18.68
	303.2	0.2108			18.66
	313.2	0.6817			18.63
	318.2	1.0897			18.61
	323.2	1.7799			18.59
4-Py	298.2	0.0843	20.71±0.27	6.04±0.86	18.91
	308.2	0.2839			18.85
	313.2	0.4926			18.82
	318.2	0.8322			18.79
	323.2	1.3595			18.76
4-Mepy	298.2	0.0592	22.99±0.61	13.03±1.98	19.10
	303.2	0.1218			19.04
	308.2	0.2356			18.97
	313.2	0.4282			18.91
	318.2	0.7189			18.84
4-^{t}bupy	298.2	0.0565	23.42±0.19	14.33±0.61	19.15
	303.2	0.1127			19.08
	308.2	0.2184			19.00
	313.2	0.4018			18.93
	318.2	0.7289			18.86
	323.2	1.318			18.79
4-DMAP	298.2	0.0244	22.34±0.90	9.19±2.90	19.60
	303.2	0.0515			19.55
	308.2	0.1047			19.51
	313.2	0.1874			19.46
	318.2	0.3144			19.42
	323.5	0.5003			19.37
4-PMe$_3$	298.2	0.0086	26.59±0.57	21.26±1.83	20.25
	308.2	0.04			20.04
	313.2	0.0853			19.93
	318.2	0.1626			19.83
	323.2	0.2911			19.72

Eyring plots

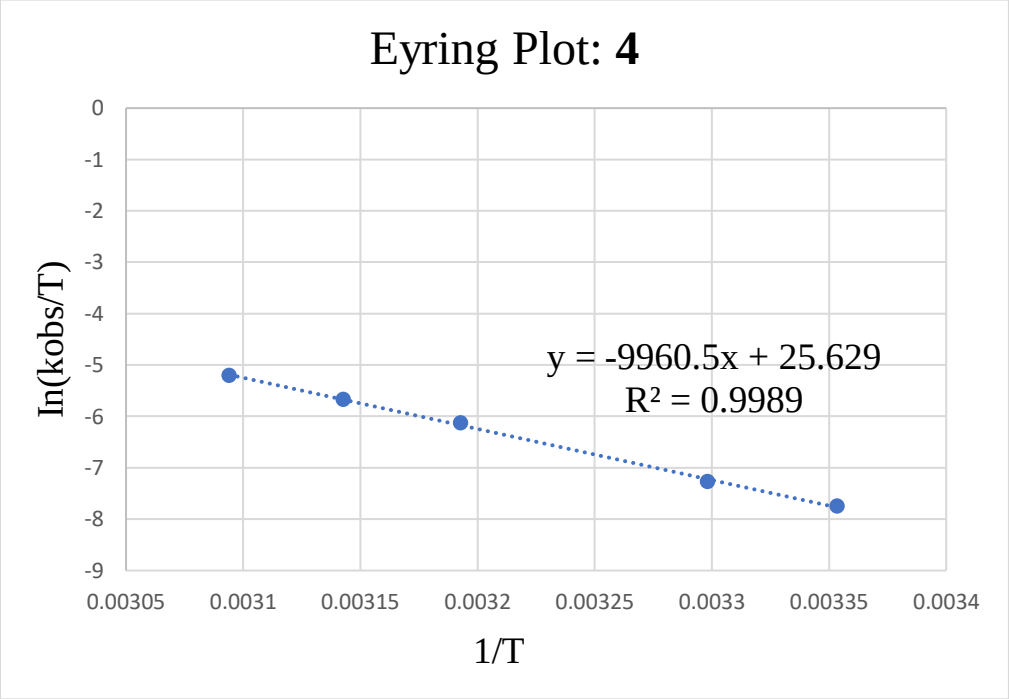

Figure 3-33. Eyring plot for **4** in $CDCl_3$.

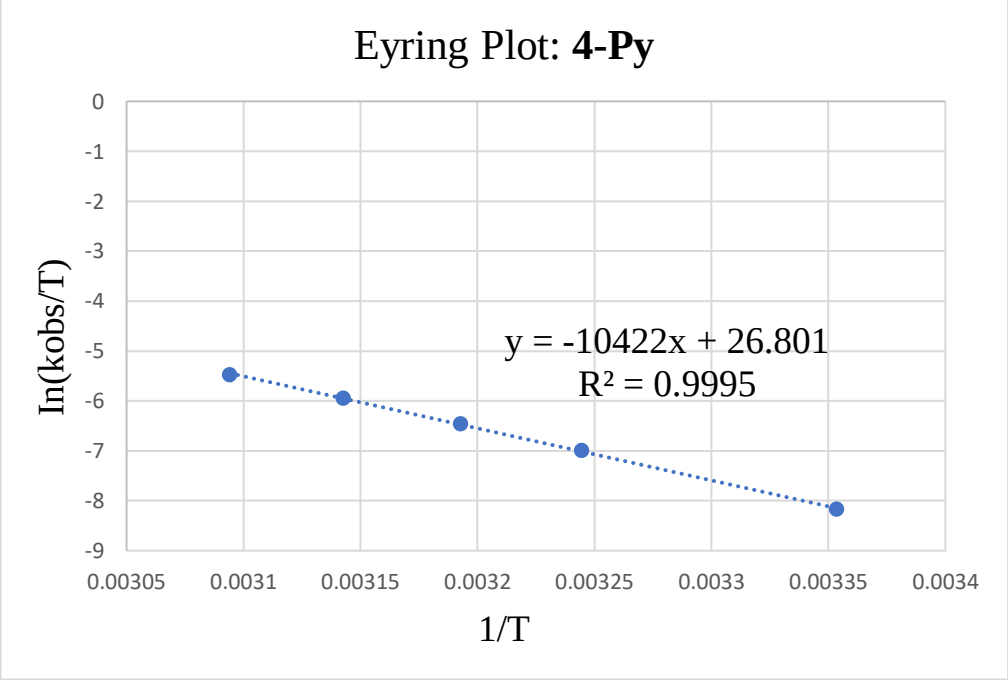

Figure 3-34. Eyring plot for **4-Py** in $CDCl_3$.

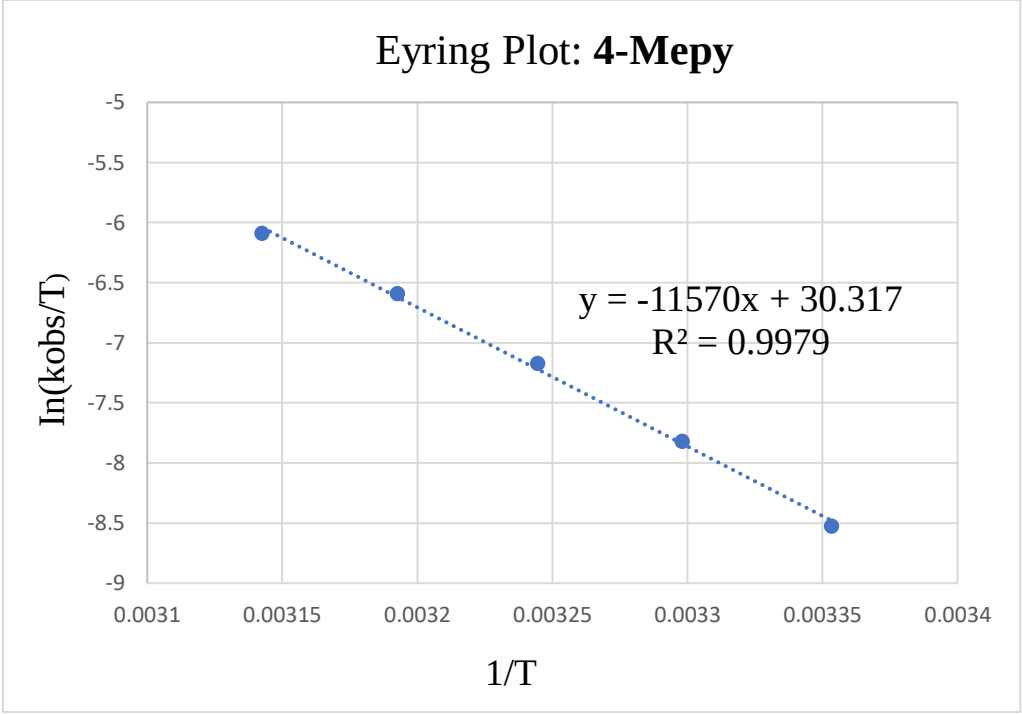

Figure 3-35. Eyring plot for **4-Mepy** in $CDCl_3$.

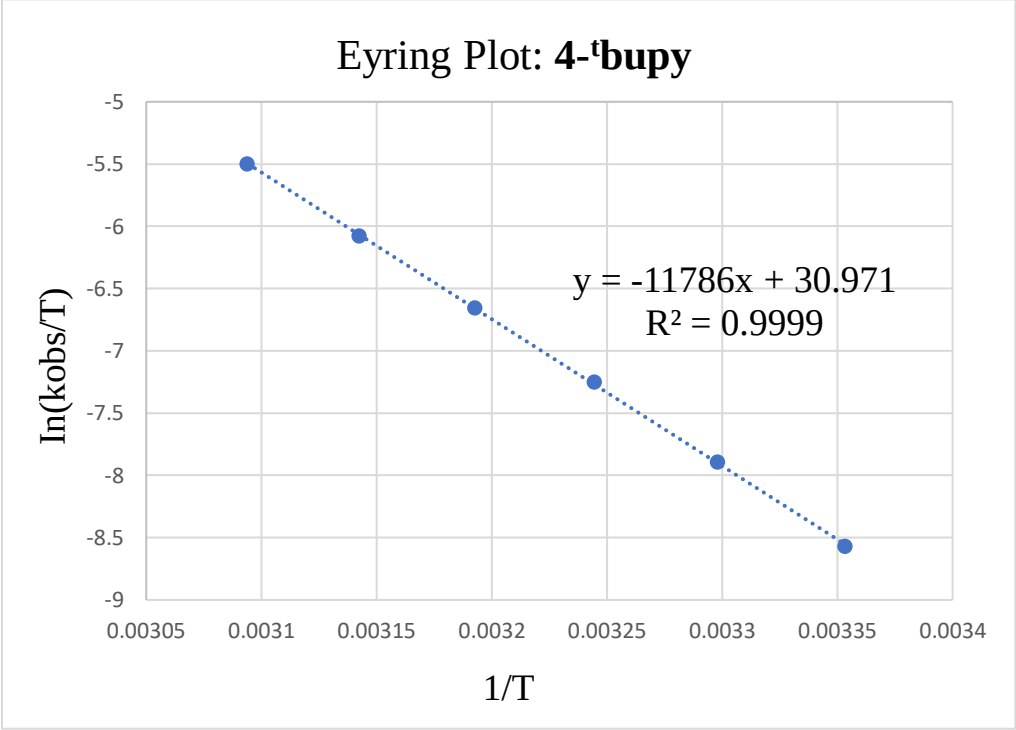

Figure 3-36. Eyring plot for **4-^{t}bupy** in $CDCl_3$.

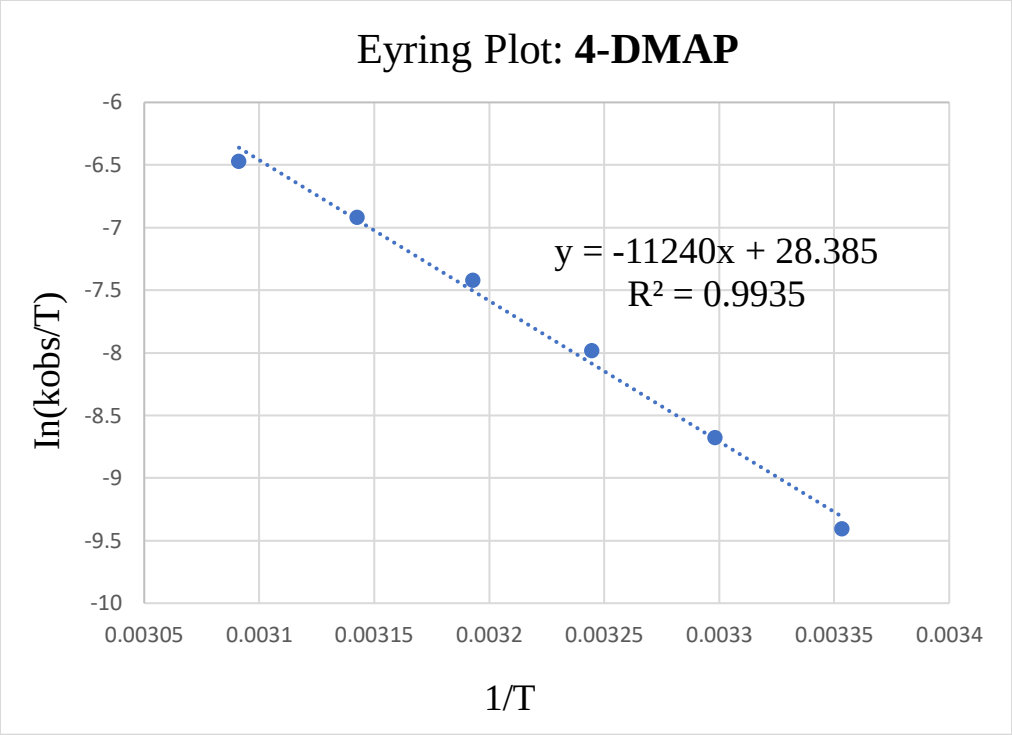

Figure 3-37. Eyring plot for **4-DMAP** in $CDCl_3$.

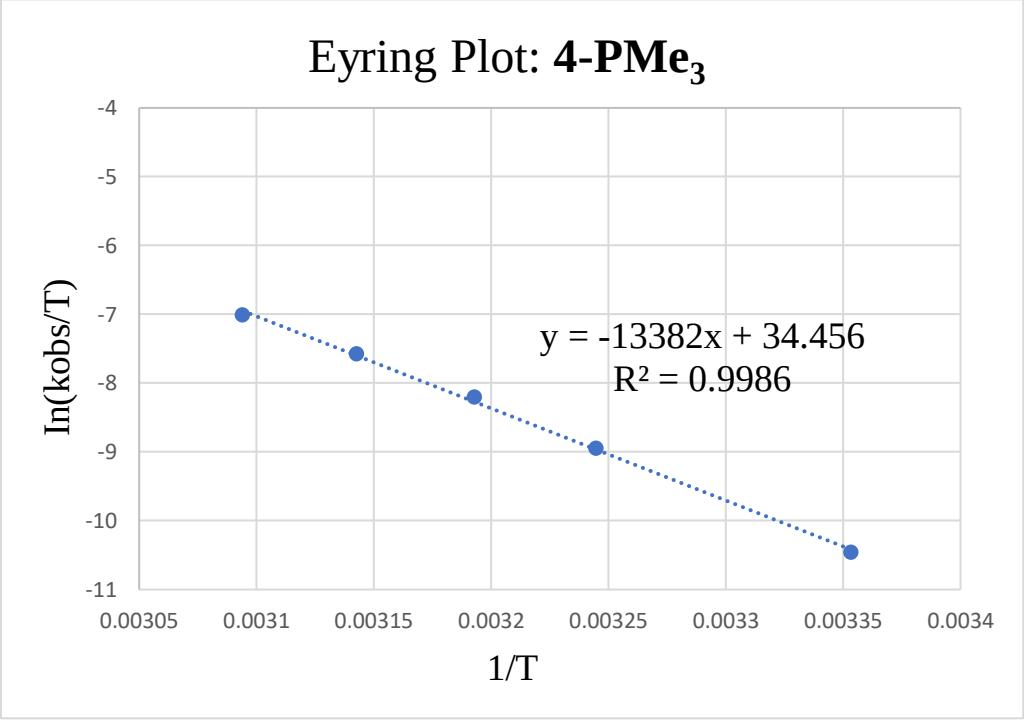

Figure 3-38. Eyring plot for **4-PMe$_3$** in $CDCl_3$.

REFERENCES

(1) Willing, W.; Christophersen, R.; Müller, U.; Dehnicke, K. VNCl2(Pyridin)2 Synthese, IR-Spektrum und Kristallstruktur. *Z. Anorg. Allg. Chem.* **1987**, *555* (12), 16–22.

(2) Critchlow, S. C.; Lerchen, M. E.; Smith, R. C.; Doherty, N. M. Vanadium Nitride Linear Chain Polymers and Monomers. Synthesis and Structures of [V(.Mu.-N)Cl2(Py)2].Infin. and V(N)Cl2(Quin)2. *J. Am. Chem. Soc.* **1988**, *110* (24), 8071–8075.

(3) Niemann, A.; Bossek, U.; Haselhorst, G.; Wieghardt, K.; Nuber, B. Synthesis and Characterization of Six-Coordinate Nitrido Complexes of Vanadium(V), Chromium(V), and Manganese(V). Isolation of a Dinuclear, Mixed-Valent μ-Nitrido Chromium(III)/Chromium(V) Species. *Inorg. Chem.* **1996**, *35* (4), 906–915.

(4) Tran, B. L.; Pink, M.; Gao, X.; Park, H.; Mindiola, D. J. Low-Coordinate and Neutral Nitrido Complexes of Vanadium. *J. Am. Chem. Soc.* **2010**, *132* (5), 1458–1459.

(5) Song, J.-I.; Gambarotta, S. Preparation, Characterization, and Reactivity of a Diamagnetic Vanadium Nitride. *Chemistry* **1996**, *2* (10), 1258–1263.

(6) Brask, J. K.; Durà-Vilà, V.; Diaconescu, P. L.; Cummins, C. C. Vanadium Nitride Functionalization and Denitrogenation by Carbon Disulfide and Dioxide. *Chem. Commun. (Camb.)* **2002**, No. 8, 902–903.

(7) Brask, J. K.; Fickes, M. G.; Sangtrirutnugul, P.; Durà-Vilà, V.; Odom, A. L.; Cummins, C. C. Niobium and Vanadium Iminophosphinimide Complexes. *Chem. Commun. (Camb.)* **2001**, No. 17, 1676–1677.

(8) Henderson, R. A.; Janas, Z.; Jerzykiewicz, L. B.; Richards, R. L.; Sobota, P. Vanadium Phenoxide Complexes with Oxide, Nitride or Hydrazide Co-Ligands: Preparation and Crystal Structures of $[V(OC_6H_3Pr^i_2\text{-}2,6)_3NLi(C_4H_8O)_3]$, $[\{VO_2(OC_6H_3Pr^i_2\text{-}2,6)_2\}_2\{\mu\text{-}Li(C_4H_8O)_2\}_2]$ and $[V(NNMe_2)(OC_6H_3Pr^i_2\text{-}2,6)_3]$. *Inorganica Chim. Acta* **1999**, *285* (2), 178–183.

(9) Farrell, W. S. Vanadium-Catalyzed Cross Metathesis: Limitations and Implications for Future Catalyst Design. *Organometallics* **2019**, *38* (19), 3481–3485.

(10) Farrell, W. S.; Greene, C.; Ghosh, P.; Warren, T. H.; Zavalij, P. Y. Decomposition of Vanadium(V) Alkylidenes Relevant to Olefin Metathesis. *Organometallics* **2020**, *39* (21), 3906–3917.

(11) Belov, D. S.; Tejeda, G.; Tsay, C.; Bukhryakov, K. V. Ring-Closing Olefin Metathesis Catalyzed by Well-Defined Vanadium Alkylidene Complexes. *Chemistry* **2021**, *27* (14), 4578–4582.

(12) Witt, M.; Roesky, H. W.; Noltemeyer, M. Synthesis and Structural Characterization of P-Functionalized Metallacyclophosphazenes. *Inorg. Chem.* **1997**, *36* (16), 3476–3479.

(13) Becker, F. N-Substituierte Tris(trimethylsiloxy)vanadin(V)-imine. *J. Organomet. Chem.* **1973**, *51*, C9–C10.

(14) Bouwkamp, M. W.; Batinas, A. A.; Witte, P. T.; Hubregtse, T.; Dam, J.; Meetsma, A.; Teuben, J. H.; Hessen, B. Relative Reactivity of the Metal−Amido versus Metal−Imido Bond in Linked Cp-Amido and Half-Sandwich Complexes of Vanadium. *Organometallics* **2008**, *27* (16), 4071–4082.

(15) Schweda, E.; Scherfise, K. D.; Dehnicke, K. Trimethylsilyl-imido-Vanadiumtrichlorid, Me3Si-N≡VCl3 Synthese, Eigenschaften und Kristallstruktur. *Z. Anorg. Allg. Chem.* **1985**, *528* (9), 117–124.

(16) DiFranco, S. A.; Maciulis, N. A.; Staples, R. J.; Batrice, R. J.; Odom, A. L. Evaluation of Donor and Steric Properties of Anionic Ligands on High Valent Transition Metals. *Inorg. Chem.* **2012**, *51* (2), 1187–1200.

(17) Coan, P. S.; Streib, W. E.; Caulton, K. G. A Triangular Heterometallic Siloxide Containing Barium. *Inorg. Chem.* **1991**, *30* (26), 5019–5023.